DYNAMICS OF SPIN TEXTURES

ALESSIO POZZI

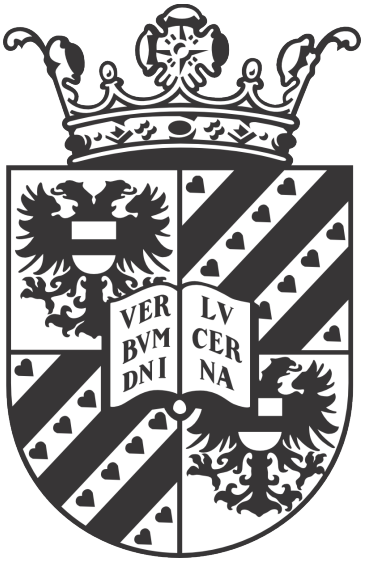

A Study of Current-Induced Motion of Magnetic Skyrmions

July 2014

university of groningen / faculty of mathematics and natural sciences / zernike institute for advanced materials

SUPERVISOR:
Prof. Dr. Maxim V. Mostovoy

REFEREE:
Prof. Dr. Tamalika Banerjee

MASTER OF SCIENCE PROGRAMME:
Top Master Programme in Nanoscience

INSTITUTE:
Theory of Condensed Matter group
Zernike Institute for Advenced Materials
Faculty of Mathematics and Natural Sciences
University of Groningen

LOCATION:
Groningen – The Netherlands

Dedicato alla mia familia.
Anche se lontana fisicamente, essa è sempre nel mio cuore.

ABSTRACT

Magnetic Skyrmions are non-coplanar nano-sized spin structures, similar to tiny knots. First observed in 2009, they were found to have highly unusual physical properties, which make them suitable for spintronics applications. Being very small and highly mobile, Skyrmions can be used as building blocks of a new generation of low-dissipation data processing and memory devices. The unusual dynamics of Skyrmions driven by electrical and thermal currents is directly related to their non-trivial topology and its understanding is of fundamental importance. Theoretical descriptions of Skyrmions that have been developed so far rely on continuous approximation of the spin textures or on adiabatic conditions of the motion of spin-polarized electrons in the non-coplanar magnetic system. The work performed in our theoretical research is aimed at developing a discrete theory of Skyrmion motion from microscopic models, considering also quantum effects, which become particularly important for nanometre-sized Skyrmions. Numerical simulations of the dynamics of single Skyrmions stabilized by frustrated exchange interactions on a triangular lattice excited by an in-plane spin-polarized current were also performed, showing evidence of the Skyrmion Hall Effect.

ACKNOWLEDGMENTS

I would like to thank my supervisor Prof. Dr. M. V. Mostovoy for the opportunity he gave me to perform my master research project. I have learnt a lot from his guidance and help through this year, and I am looking forward to continuing working with him for my PhD. I also thank Dr. A. Leonov for the helpful discussions we had about some aspects of the numerical simulations.

I acknowledge the Zernike Institute for Advanced Materials for financial support of my studies.

I am particularly grateful to my family, mum Tiziana, dad Amleto and my two brothers Daniele and Francesco: their support from back home has been essential for the achievement of this important goal. Last but not least, I am most thankful to my life partner Sara. She helped me in every difficult moment, including (and particularly) during this last thesis-writing period.

RINGRAZIAMENTI

Vorrei ringraziare il mio relatore Prof. Dr. M. V. Mostovoy per avermi dato l'opportunità di svolgere la mia ricerca di tesi magistrale. Quest'anno ho imparato molto dalla sua supervisione, e sono felice di continuare il lavoro con lui per il mio PhD. Ringrazio anche il Dr. A. Leonov per le utili conversazioni riguardo alcuni aspetti delle simulazioni numeriche.

Ringrazio lo Zernike Institute for Advanced Materials per il supporto economico dei miei studi durante questi due anni.

Sono particolarmente grato verso la mia familia, mamma Tiziana, papà Amleto e i miei due fratelli Daniele e Francesco: il loro supporto (così come quello della mia familia intera) da giù in Italia è stato fondamentale per il raggiungimento di quest'obiettivo. Infine, rivolgo un ringraziamento speciale alla mia compagna di vita Sara. Grazie a lei sono riuscito a superare i momenti più difficili, incluso (e soprattutto) quest'ultimo periodo di scrittura della tesi.

CONTENTS

LISTINGS

ACRONYMS

SkX	Skyrmion Crystal
DM	Dzyaloshinskii–Moriya
LTEM	Lorentz Transmission Electron Microscopy
srSTM	spin-resolved Scanning Tunneling Microscopy
FM	ferromagnetic
AFM	antiferromagnetic
nn	nearest-neighbour
nnn	next-nearest-neighbour
THE	Topological Hall Effect

SHE Skyrmion Hall Effect

TmHE Topological magnon Hall effect

GMR Giant Magneto-Resistance

CM Center of Mass

LLG Landau-Lifshitz-Gilbert

1 INTRODUCTION

Skyrmions take their name from the British nuclear physicist T.H.R. Skyrme [1], who introduced them in the early 60's as a soliton solution of the non-linear sigma model to describe mesons and baryons in a unified theory. In his original work, Skyrme considered three-dimensional versions of Skyrmions, but later the definition was expanded to account for more general theories. A Skyrmion is a smooth, topologically stable field configuration which defines a non-trivial surjective mapping from real space (or momentum space) to an order parameter space with a non-trivial topology. Furthermore, a Skyrmion is everywhere non-singular, finite and trivial at infinity, i. e. it has no winding at infinity.

With the advent of Quantum chromodynamics, Skyrmions went out of the focus of the scientific community for about twenty years. It is in the seemingly unrelated field of Solid State Physics that they made their reappearance in the late 80's, when Bogdanov and Yablonskiy theoretically predicted the existence of spin structures similar to Skyrmions in non-centrosymmetric magnetic materials [2]. In this type of Skyrmions the order parameter is magnetization, while the dimension is dictated by the physical dimensions of the considered problem and materials.

Following these pioneering theoretical works, several experimental groups have recently found Skyrmions in magnetic materials (ferromagnets, multiferroics and ferrimagnets) using a variety of techniques such as neutron scattering [3], Lorentz Transmission Electron Microscopy (LTEM) [4] and spin-resolved Scanning Tunneling Microscopy (srSTM) [5].

1.1 GENERAL PROPERTIES OF SKYRMIONS

In the context of condensed matter physics, magnetic Skyrmions, or simply Skyrmions, are particle-like nanometre-sized spin textures with a non-trivial topology that guarantees their stability against perturbations. A single Skyrmion is shown in figure 1.1, where arrows represent spins. Skyrmions are stable in the sense that they are topologically protected: they are characterized by a topological integer number that cannot be changed by a continuous deformation of the spin configuration. The topological Skyrmion number (or topological charge),

$$Q = \frac{1}{4\pi} \iint d^2 r \, \mathbf{n} \cdot (\partial_x \mathbf{n} \times \partial_y \mathbf{n}) \,, \tag{1.1}$$

Figure 1.1: An isolated Skyrmion. The spin orientation is indicated by arrows.

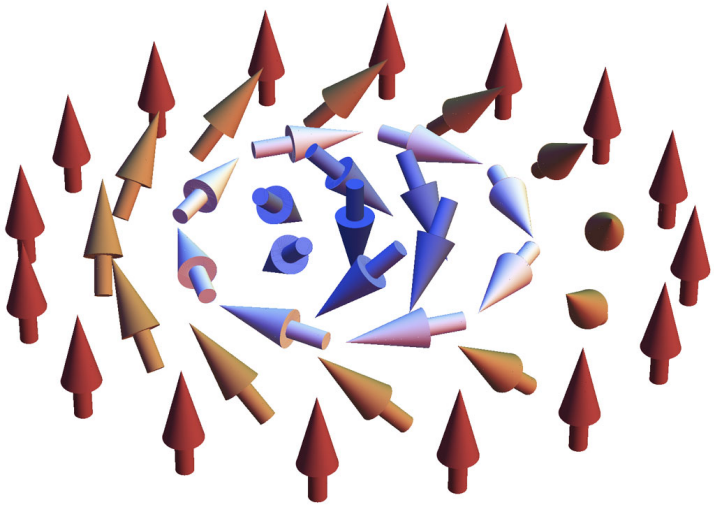

counts how many times the unit vector $\mathbf{n}(\mathbf{r})$ in the direction of magnetization wraps around a unit sphere [6, 7] (see also Appendix A.1). For a single Skyrmion $Q = \pm 1$. In addition to the topological charge, Skyrmions are characterized by chirality and helicity (see figure 1.2). So far, only the Skyrmions with the chirality $m = \pm 1$ and helicity $\gamma = \pm \pi/2$ have been observed. The definition of m and γ can be found in Appendix A.2).

Skyrmions appear in the ground state of several magnetic materials in some interval of temperatures and magnetic fields. How extended the region of Skyrmion phase is depends on the interactions stabilizing these spin textures and on the dimensionality of the magnetic material. Most Skyrmion phases in bulk materials only exist in a tiny pocket of the phase diagram near the transition temperature. The phase diagram of bulk MnSi with the region where Skyrmion crystals are formed is shown in figure 1.3. Thin films, nanoribbons and similar confined-geometry nano-structures, on the other hand, show phase diagrams with wider Skyrmion phases extending to low temperatures and low applied magnetic fields (see for example the phase diagram of thin film $Fe_{0.5}Co_{0.5}Si$ shown in figure 1.4).

Four mechanisms leading to the Skyrmion state have been identified so far:

1. Long range magnetic dipolar interactions;
2. Dzyaloshinskii–Moriya (DM) interactions;
3. Four-spin exchange interactions (and in general more exotic exchange interactions);
4. Frustated exchange interactions.

Figure 1.2: Different Skyrmion structures with varying vorticity m and helicity γ. The arrows and colours represent in-plane spin directions, while the brightness indicates the component normal to the plane (white = up, black = down).

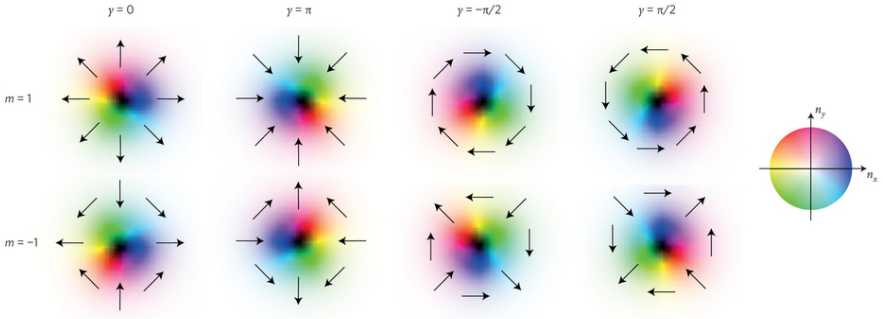

Figure 1.3: A: Phase diagram of MnSi at ambient pressure as a function of T and B [3]. Experimental points show boundaries between the different phases. The A-phase, shown schematically in the panel B, is characterized by a crystal of skyrmions.

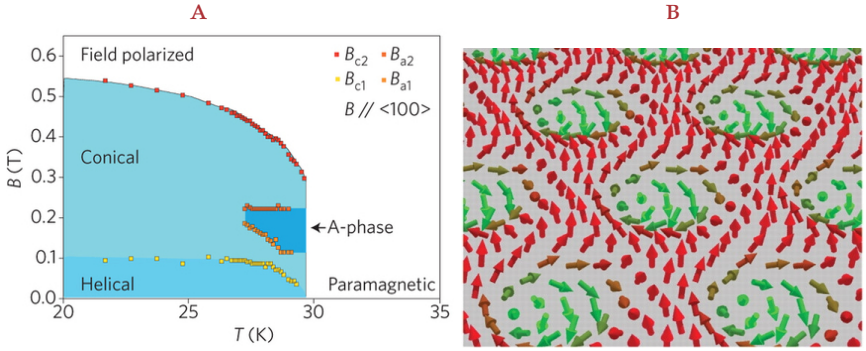

Figure 1.4: Observed phase diagram of $Fe_{0.5}Co_{0.5}Si$ thin film in the B–T plane [4]. The colour bars indicate the skyrmion density per 10^{-12} m². Dashed lines show the phase boundaries between the skyrmion crystal (SkX), spiral (H) and FM phases.

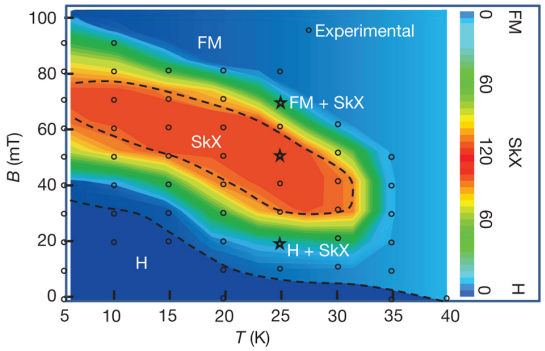

Long range magnetic dipolar interactions are crucial for the formation of magnetic bubbles, some of which have the topology of Skyrmions, in magnetic thin films with a perpendicular easy-axis anisotropy. The dipolar interactions favour an in-plane magnetization thus competing with the uniaxial anisotropy and resulting in a periodic stripe domain spin structure where the regions of up and down magnetization are separated by Bloch walls. An applied magnetic field results in the formation of cylindrical domains (or magnetic bubbles) with the topology of Skyrmions [8]. Since the magnetodipolar interactions are relatively weak, the Skyrmions in thin magnetic films have typical dimensions of 100–1000 nm.

Another mechanism for the formation of Skyrmions is the antisymmetric Dzyaloshinskii–Moriya interaction

$$H_{DM} = \mathbf{D}_{12} \cdot \mathbf{S}_1 \times \mathbf{S}_2.$$

It originates from the relativistic spin-orbit coupling and is present in many magnetic systems, often resulting in a small canting of spins (e.g., weak ferromagnetism of antiferromagnets). The DM interaction becomes particularly important in magnets whose crystal lattice lacks inversion symmetry. In this case, terms linear in gradient of magnetization, e. g.the Lifshitz invariant

$$\mathcal{L} = D\,(\mathbf{n} \cdot \nabla \times \mathbf{n})$$

are allowed by symmetry in the phenomenological expression of the free energy, resulting in a coherent rotation of the spins. Thus the DM interaction in non-centrosymmetric magnets transforms a uniform magnetic state into a helical spiral. An applied magnetic field favours a state with three coexisting spirals, which is the Skyrmion Crystal (SkX) state. SkX phases in non-centrosymmetric magnets have been experimentally observed in MnSi [3], $Fe_{1-x}Co_xSi$ [9], FeGe [10] and $Mn_{1-x}Fe_xGe$ [11]. The size of Skyrmions stabilized by DM interactions is in the range of $5 - 100$ nm. As this size is inversely proportional to the coupling constant D, materials with a higher value of D host smaller Skyrmions. For example, Skyrmions formed in MnGe have a radius of ~ 3 nm.

The four-spin exchange interaction occurs due to electron hopping between four adjacent sites (ring exchange). Its coupling constant is usually smaller than the Heisenberg exchange constant J and its contribution to the energy is often ignored. Nevertheless, there are systems where the four-spin exchange interaction plays an important role in the formation of complex magnetic structures. For example, Heinze *et al* [5] investigated the formation of Skyrmions in hexagonal Fe films of one-atomic-layer thickness on the Ir(111) surface. Here the four-spin exchange interaction can compete with the exchange energy, as the nearest-neighbour (nn) ferromagnetic (FM) exchange coupling

Figure 1.5: A–D: Illustration of a spin spiral and Skyrmions of different rotational senses and topological charge Q. A: 90° spin spiral (Q = 0); B: clockwise Skyrmion (Q = +1); C: antiSkyrmion (Q = −1); D: anticlockwise Skyrmion (Q = +1). The size and sign of the four-spin interaction term is indicated by black numbers for different diamonds (shaded areas) consisting of four adjacent lattice sites (ijkl). The in-plane projection of the Dzyaloshinskii–Moriya (DM) vector **D**, which couples spins on adjacent sites, is also given by red arrows for pairs of nearest neighbours. The value of the DM term is indicated by red numbers. Adopted from ref. [5].

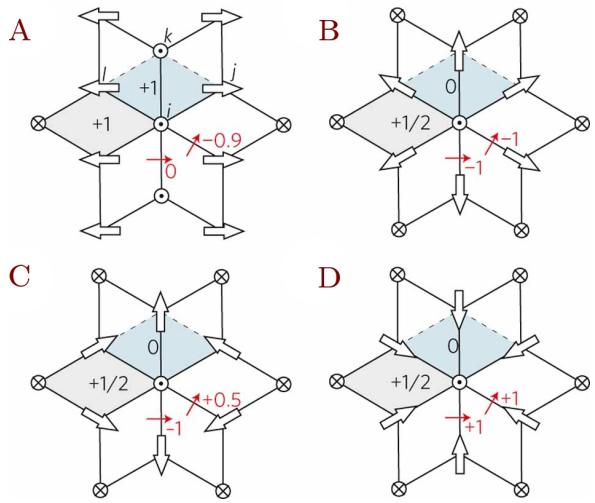

is unusually small for Fe/Ir(111) due to the strong Fe − Ir hybridization. The four-spin interaction plays a crucial role in coupling different spin spirals (1D) into two-dimensional magnetic structures, but also DM interactions are important in such materials, as they lower the energy of the Skyrmion (Q = +1) and antiSkyrmion (Q = −1) lattices with respect to the multi-spiral state (see figure 1.5). Skyrmions resulting from such interactions are very small. Their size is comparable to the period of the underlying lattice.

Skyrmions have been theoretically predicted to form also in systems with competing Heisenberg exchange interactions, e.g. in triangular ferromagnets with next-nearest-neighbour (nnn) antiferromagnetic (AFM) interactions. The absence of inversion symmetry of the crystal lattice is not required for this mechanism [12] Skyrmions in such frustrated magnetic materials would be very small in size (~lattice constant) and present many degeneracies: in contrast to the case of DM-stabilized Skyrmions, where the chirality and helicity are fixed by the sign of D, here the formation of Skyrmions of any of the types shown in figure 1.2 is possible. Unfortunately, to date, no frustrated materials satisfying the right properties have been experimentally synthesized, leaving the research opportunities to find new Skyrmion materials wide open.

We shall see how the magnetic ground state of a material is found into deeper detail in the next chapter.

1.2 POSSIBLE APPLICATIONS OF SKYRMIONS

The interest of the scientific community in Skyrmions is mostly driven by the fact that Skyrmions are very promising information bits for novel types of spintronic storage and logic devices [13]. Magnetic bubble memories have been a topic of intense study in the 70's and are now used for niche applications. The research on manipulation of Skyrmions is becoming very active, and a number of encouraging results is increasing the confidence of scientists that one day Skyrmions will be implemented in devices useful to everyone. Today's hard-disk drives already achieve high densities of storage, but the increasing complexity and fragility of their mechanical parts motivate the need for solid state devices with comparable or even higher bit densities. The prime example of such devices [14] is based on ferromagnetic domains (spin up or spin down), separated by domain walls and located on a magnetic nano-ribbon in a train fashion. The train of domain walls can be moved electrically through the spin torque, thus making it possible to read and write magnetic bits. However, there are some problems with this technology. Namely, the critical current densities necessary to depin domain walls are too high, resulting in too much energy consumption and dissipation. Furthermore, the dimension of the magnetic domains cannot be made smaller than about 50 nm, rendering this approach still too far from the transition to a competitive technology.

Skyrmions might help to solve most of these issues. Joniets *et al* have demonstrated that the critical currents needed to move Skyrmions are about six orders of magnitude smaller than the ones needed to move domain walls [15], suggesting that the Skyrmion-based devices would have much lower power consumption. Moreover, Skyrmions that can be as small as a few nanometres (and in principle, even comparable to interatomic spacing) can potentially provide an ultra-high information-storage density.

Significant challenges still have to be met before Skyrmionic devices can become a reality. All the studied Skyrmion systems, for example, show a crystal of Skyrmions at low temperatures (up to 250 K). For memory applications though, we would need to be able to manipulate single Skyrmions at room temperature. To tackle this issue, Fert, Cros and Sampaio have recently shown through micro-magnetic simulations that layered structures of high-T_c materials and surface-induced DM interactions can stabilize Skyrmions at room temperature [16]. A significant step forward for the realization of Skyrmion writing/deleting processes was made at the University of Hamburg, where PhD student Romming and co-workers were able to write and

delete single Skyrmions with a spin-polarized STM tip on an ultra-thin magnetic film [17].

Even lower energy consumptions could be achieved following a parallel and modern all-spin approach, named *magnonics*. The scope of this new research field (initialized in 2009 in Dresden[1]) is still under debate, but the main concept is the one to manipulate information bits with magnons instead of electrical currents. Energies involved in the dynamics of all-spin systems are much lower with respect to the conventional ones where electrical currents are used, therefore, moving the Skyrmions with magnons will be much more energetically efficient. Recently, a collaboration between the University of Groningen and *RIKEN (Japan)* found that magnon currents can force Skyrmions to rotate in a Feynman's ratchet-like fashion, suggesting that magnons can indeed be used to control the motion of these spin textures [18].

1.3 SKYRMION DYNAMICS AND NEW TOPOLOGICAL EFFECTS

The non-coplanar Skyrmion spin configuration brings about some novel and intriguing physics, in particular, when we consider the propagation of spin-polarized electrons through Skyrmions. Understanding electron-Skyrmion interactions is very important for the control of Skyrmions with electrical currents.

When a spin polarized electron propagates through the spin texture of a Skyrmion, its wave function gains a Berry phase deriving from the non-trivial Skyrmion topology. This phase happens to coincide with the phase gained by the wave function of a charged particle propagating in a magnetic field. Therefore, effectively the Skyrmion acts on electrons as a flux ϕ of magnetic field. Moreover, this magnetic flux is quantized:

$$\phi = Q\phi_0,$$

where

$$\phi_0 = \frac{hc}{e}$$

is the elementary magnetic flux.

The resulting effective gauge potential for electrons is

$$a_\mu = \frac{1}{2}(1 - \cos\Theta)\,\partial_\mu \Phi,$$

where Θ and Φ are the spherical angles describing the direction of the local magnetization [19] and μ is the space-time index. The 4-vector

1 The first magnonics conference, entitled 'Magnonics: From Fundamentals to Applications' was held in Dresden in August 2009, sponsored by the visitor programme of the Max Planck Institute for the Physics of Complex Systems (MPIPKS).

Figure 1.6: Artist-impression of a single electron moving through a Skyrmion in the adiabatic approximation, in which the electron spin aligns perfectly with the local magnetic moment. This interaction gives rise to the Berry phase gauge potential a_μ. Adopted from [20].

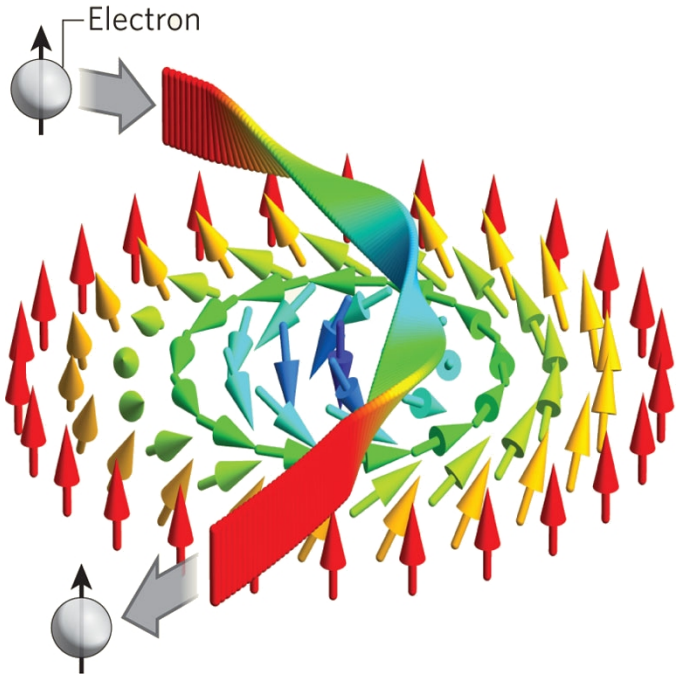

potential $a = (a_0, \mathbf{a})$ gives rise to internal electric and magnetic fields, $\boldsymbol{e}$ and $\mathbf{b}$: just like in the case of the electromagnetic vector potential $\boldsymbol{A}$,

$$\mathbf{b} = \nabla \times \mathbf{a}$$

and

$$\boldsymbol{e} = -\nabla a_0 - \partial_0 \mathbf{a}.$$

It is important to notice that these effective fields are often very strong. An estimate of the magnitude of $\mathbf{b}$ is

$$\langle b \rangle \sim \frac{\phi_0}{\pi R_0^2},$$

where R_0 is the radius of the Skyrmion. Thus the smaller the Skyrmions, the larger the fields. For MnSi with $R_0 \sim 18\,\text{nm}$ the effective magnetic field is about 20 T, while for MnGe with $R_0 \sim 3\,\text{nm}$ it is about 400 T.

When electrons pass through a static Skyrmion (see figure 1.6), their motion is affected by the magnetic field $\mathbf{b}$. When the current is higher than some critical pinning value, the Skyrmions gain a momentum from the electrons and generate an electric field $\boldsymbol{e}$, which in

Figure 1.7: Artist impression of topological phenomena related to Skyrmions. Adopted from [24].

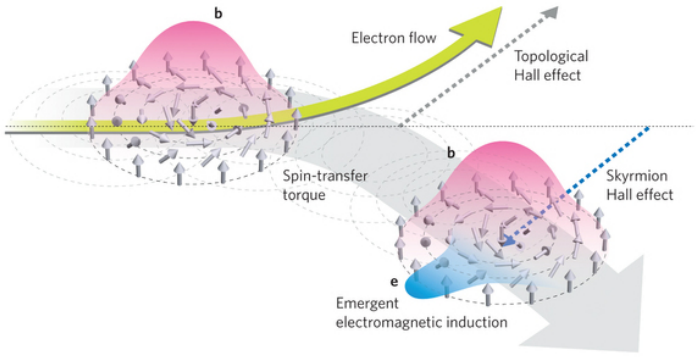

turn also affects the motion of electrons. A deep understanding of this coupled electron-Skyrmion dynamics is of fundamental importance for the field, both from the applied and the theoretical points of view, and most of the ongoing research today focuses on this issue.

Depending on the sign of the Skyrmion topological charge, electrons passing through a Skyrmion are scattered to the left or to the right, giving rise to a novel type of Hall effect, the Topological Hall Effect (THE) (see figure 1.7). It was shown that the Hall resistivity ρ_{xy} decreases with increasing velocity of the Skyrmions [21, 22]. Indeed the velocity of moving Skyrmions can be measured exploiting such a dependence. Another Hall effect resulting from the Gilbert damping of Skyrmions, is the Skyrmion Hall Effect (SHE), i. e. the motion of Skyrmions in the direction normal to the applied electrical current [23]. The Topological magnon Hall effect (TmHE) has also been measured and theoretically modelled recently [18].

While the emerging electromagnetic fields from the electron-skyrmion interactions resemble the usual electromagnetic fields, the dynamics of Skyrmions is highly unusual. In particular, the Y coordinate of the Skyrmion plays the role of momentum for the X coordinate, and *vice versa*, i. e. there is a canonical conjugate relation between the X and Y coordinates of the Skyrmion. Another unusual consequence of the non-trivial Skyrmion topology, is the fact that the Skyrmion velocity is perpendicular to the force applied to it. This results in the gyroscopic motion of Skyrmions.

In Chapter 3 we shall describe how spin textures interact with electrical currents, revising some of the most established models and developing a discrete model for non-smooth spin textures. Most of the problems treated in this thesis lead to non-solvable (differential) equations, therefore numerical methods were extensively applied. In chapter 4 such methods are discussed, along with the results obtained. Finally, in the last chapter we draw our conclusions and suggest paths to continue and improve this research.

2

GINZBURG-LANDAU THEORY, MECHANISMS AND MATERIALS

In this chapter we will discuss a theoretical method to find the equilibrium magnetization ordering of a system given the symmetries of a material and an applied magnetic field at a certain temperature. In the first section we will revise a type of antisymmetric interaction which is crucial in the formation of non-collinear magnetic orders. In the following sections, the continuous theory of phase transitions will be deepened and the phase diagram of MnSi will be modelled through this theory. Finally, in the last section, we shall consider those cases where a continuous model for magnetization is not applicable and hence study some non-trivial microscopic models.

2.1 DZYALOSHINSKII–MORIYA INTERACTION

The Dzyaloshinskii–Moriya interaction, also referred to as the Antisymmetric interaction, is a contribution to the total exchange interaction between two neighbouring atoms with magnetic spin $\mathbf{S}_i$ and $\mathbf{S}_j$. This interaction is entirely represented by a vector $\mathbf{D}_{ij}$ (see Fig. 2.1) and is proportional to the vector product of the two spins:

$$H_{DM}^{ij} = \mathbf{D}_{ij} \cdot \mathbf{S}_i \times \mathbf{S}_j. \tag{2.1}$$

It arises in molecules or crystals which lack inversion symmetry. Originally introduced with a phenomenological approach by Dzyaloshinskii [25] following symmetry arguments based on Landau Theory, it

Figure 2.1: Dzyaloshinskii–Moriya $\mathbf{D}_{ij}$ vector representing the antisymmetric interaction between spins $\mathbf{S}_i$ and $\mathbf{S}_j$ deriving from spin-orbit coupling and mediated by a single third ion (ligand) by the superexchange mechanism. Adopted from wikipedia.

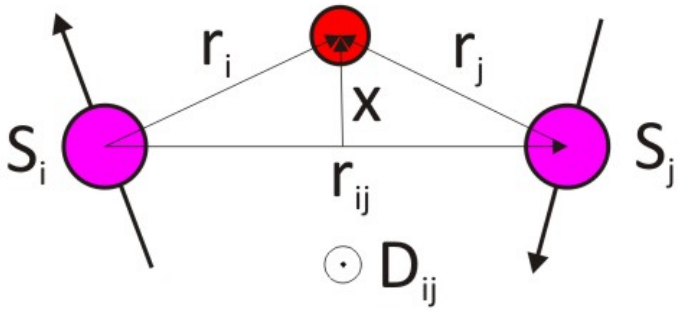

was derived microscopically by Moriya [26] by a pertubative treatment of the spin-orbit coupling term. Its effect, in combination with FM (AFM) Heisenberg exchange which produces parallel (anti-parallel) alignment of spins, is to favour a coherent canting of the spins, introducing chirality in the magnetic configuration. This is what happens, for example, in the ground state of helimagnets, such as MnSi.

The orientation of the vector $\mathbf{D}_{ij}$, which affects the modulation of the spin texture, is dictated by the crystal structure. As an example, referring to the figure, in the case when the exchange is mediated by a ligand, $\mathbf{D}_{ij}$ is proportional to the vector product of $\mathbf{r}_i$ and $\mathbf{r}_j$:

$$\mathbf{D}_{ij} \propto \mathbf{r}_i \times \mathbf{r}_j = \mathbf{r}_{ij} \times \boldsymbol{x} \tag{2.2}$$

From this expression it is clear that $\mathbf{D}_{ij}$ is perpendicular to the plane determined by the three ions and vanishes when the three ions are in line.

2.1.1 *DM interaction and Lifshitz invariants*

In the context of a Landau expansion of the free energy of a field of spins with fixed magnitude $\mathbf{S}(\mathbf{r}) = S\mathbf{n}(\mathbf{r})$, the DM interaction term is represented by a combination of Lifshitz invariants. The crystallographic classes we are interested in are the ones which lack inversion symmetry, that is, C_n, S_4 and D_{2d}. However, since the interactions present in structures of the groups S_4 and D_{2d} are intrinsically anisotropic, they are not important in our scope. If we consider the crystallographic class C_n, the most general form of the Dzyaloshinskii–Moriya interaction is

$$\begin{aligned}\frac{\epsilon_{DM}}{S^2} = D_1 &\left(n_z\frac{\partial n_x}{\partial x} - n_x\frac{\partial n_z}{\partial x} + n_z\frac{\partial n_y}{\partial y} - n_y\frac{\partial n_z}{\partial y}\right)\\ + D_2 &\left(n_z\frac{\partial n_x}{\partial y} - n_x\frac{\partial n_z}{\partial y} - n_z\frac{\partial n_y}{\partial x} + n_y\frac{\partial n_z}{\partial x}\right)\\ + D_3 &\left(n_x\frac{\partial n_y}{\partial z} - n_y\frac{\partial n_x}{\partial z}\right),\end{aligned} \tag{2.3}$$

where D_i are the components of the DM vector. Considering the subgroup D_n (to which, i. e. MnSi belongs to) puts additional constraints on these, namely

$$\begin{cases} D_1 = 0, \\ D_2 = D_3 = -D, \end{cases} \tag{2.4}$$

the invariant becoming

$$\epsilon_{DM} = D\mathbf{S} \cdot \nabla \times \mathbf{S}; \tag{2.5}$$

while considering the subgroup C_{nv}, the only non-zero term is D_1.

2.2 GINZBURG-LANDAU THEORY AND PHASE DIAGRAM OF MNSI

The Ginzburg-Landau theory is a phenomenological theory for a continuum description of phase transitions. It is named after V. L. Ginzburg and L. D. Landau and can be applied to a wide range of areas in physics. The central concept of this theory is based on the existence of an order parameter that is non-zero in the ordered phase below a critical temperature T_C, and which becomes zero when increasing the temperature above T_C. Close to the phase transition the order parameter is small, so that the appropriate energy functional can be expanded as a power series in the order parameter. Minimizing this functional with respect to the order parameter yields the equilibrium thermodynamics of the system. In the case of ferromagnetism or smoothly varying magnetic textures the order parameter is the local magnetization $\mathbf{M}(\mathbf{r})$. In thermal equilibrium, the magnetic state of a system is the one that minimizes the free energy.

In this section we will focus our attention on finding magnetic orders through minimizing the Ginzburg-Landau functional for a simple case (ferromagnets) and for the description of the phase diagram of the itinerant helimagnet MnSi. This involves being able to find the appropriate energy functional depending on the symmetries of the system. The reason to study into such detail this material is that the Skyrmion lattice in a magnetic material was first observed in 2009 by Mühlbauer *et al*. [3] in such a crystal. They used neutron scattering to observe the spontaneous formation of this novel type of magnetic order. Other materials of the same B20 cubic structure family (or isometric structure) show similar H–T characteristics.

2.2.1 *Ferromagnets*

The Ginzburg-Landau free energy functional for ferromagnets obeys the following symmetries:

- Spatial translation;
- Spatial rotation;
- Spatial inversion;
- Transformation $\mathbf{M} \longrightarrow -\mathbf{M}$;
- Transformation $\mathbf{B} \longrightarrow -\mathbf{B}$;

- If $(B = 0)$: Combined rotation in space and spin space;

- If $(B \neq 0)$: Combined rotation in space and spin space, around the axis defined by $\mathbf{B}$;

It can be written in its most general form as

$$\mathcal{E} = \int d^3r \left[\alpha \mathbf{M}^2 + J(\nabla \mathbf{M})^2 + U\mathbf{M}^4 - \mathbf{B}\cdot\mathbf{M} + (\text{higher orders})\right] \quad (2.6)$$

where we have for simplicity adopted units in which the lattice constant $a = 1$ (this assumption will always be made in the following, unless differently specified). Note that here $\mathbf{M}^n$ means $\|\mathbf{M}\|^n = M^n$ and $(\nabla \mathbf{M})^2 = \partial_i M_j \partial_i M_j$. The parameters in Eq. (2.6) derive from the microscopic theory of the problem, e. g. $(J > 0)$ represents Heisenberg FM exchange and $U > 0$ mode-mode interaction to lowest order. The parameter α as we will see, is crucial for determining in what kind of phase the system is, and is temperature dependent: $\alpha(T) \propto (T - T_C)$. In the case of zero magnetic field, the functional (2.6) is minimized for homogeneous ferromagnetic configuration $(\partial_i \mathbf{M} = 0)$, and the net magnetization if found when its variation is zero:

$$\begin{aligned} \frac{\delta \mathcal{E}}{\delta \mathbf{M}} = 0 \implies \\ 2M(\alpha + 2UM^2) = 0 \implies \\ \begin{cases} M = 0 \\ M = \pm\sqrt{-\frac{\alpha}{2U}}\,. \end{cases} \end{aligned} \quad (2.7)$$

Therefore, when the temperature is below the critical temperature $(\alpha < 0)$ the system has a neat, non-zero magnetization, while the magnetization is zero (paramagnetic phase) for temperatures above T_C $(\alpha > 0)$.

2.2.2 *MnSi: Helical (H), Conical (C) and Skyrmion (A) phases*

Given the structural properties of MnSi (see Fig. 2.2 and Ref. [28]) and what we have discussed in the previous section, the free energy functional for helimagnets takes on a different general expression. In particular, the lack of inversion symmetry allows for additional terms which have odd powers of spatial derivatives and thus are odd under spatial inversion. The most important additional contribution for helimagnets is the DM term

$$\mathcal{E}_{DM} = \int d^3r\, D\mathbf{M}\cdot(\nabla \times \mathbf{M}). \quad (2.8)$$

As we will see, the sign of D determines the chirality of the resulting magnetic order (e. g. $D > 0 \implies$ left-handed spiral), while the ratio

Figure 2.2: The B20 crystal structure of MnSi, showing one unit cell. Adopted from [27]

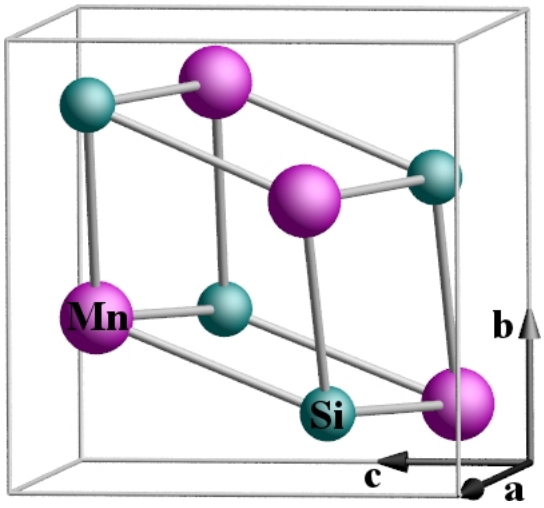

of the strength of the DM interaction coupling (that forces a canted order) and ferromagnetic coupling (which instead prefers a parallel order) fixes the wavelength (or, more generally, the length scale ξ) of such magnetic structures.

HELICAL AND CONICAL ORDERS Consider the free energy functional

$$\mathcal{E} = \int d^3r \left[\frac{J}{2}(\nabla \mathbf{M})^2 + D\mathbf{M} \cdot (\nabla \times \mathbf{M}) - \mathbf{B} \cdot \mathbf{M} \right]. \tag{2.9}$$

As we can see in Fig. 1.3–A, below a certain critical temperature ($T_C \sim 29\,K$), for zero magnetic field (or very low magnetic field) MnSi shows an helical magnetic ordering. Let us for simplicity consider just the case of zero field. It is reasonable then to 'guess' a solution of the type

$$\mathbf{M}(\mathbf{r}) \propto \hat{e}_1 \cos(\mathbf{Q} \cdot \mathbf{r} + \varphi) + \hat{e}_2 \sin(\mathbf{Q} \cdot \mathbf{r} + \varphi), \tag{2.10}$$

where $\hat{e}_1$ and $\hat{e}_2$ are two orthonormal vectors and $\mathbf{Q}$ is the wave vector of the spiral. This expression can describe, with the proper choice of $\mathbf{Q}$, a helical or cycloidal spiral and also a ferromagnetic state ($Q = 0$). Plugging this solution into (2.9) the free energy becomes

$$\mathcal{E} \propto \int d^3r \left[\frac{J}{2} Q^2 - D\mathbf{Q} \cdot \hat{e}_1 \times \hat{e}_2 \right], \tag{2.11}$$

which is minimized for $\mathbf{Q}$ parallel to $\hat{e}_3$ and

$$\begin{aligned} &\frac{\delta \mathcal{E}}{\delta Q} = 0 \implies \\ &Q = \frac{D}{J} \qquad \text{(in units of } a^{-1}\text{)}. \end{aligned} \tag{2.12}$$

The inverse wavevector corresponds to the length scale on which the magnetic structures develop:

$$\xi = \frac{J}{D} \qquad \text{(in units of } a\text{)}. \tag{2.13}$$

As expected ξ is determined by J and D. The weaker the DM interaction with respect to the FM exchange, the smaller the wave vector Q, that corresponds to longer modulations of the magnetization.

In Eq. (2.9) we have neglected some higher order terms that nevertheless are not crucial in the description of the conical and Skyrmion phases:

- $\mathbf{M}^4$ and $(M_x^4 + M_y^4 + M_z^4)$ These terms determine the direction of the magnetization vectors related to the direction of the cubic crystal axes;

- $(\partial_i M_i)^2$ These terms fix the direction of wave vector $\mathbf{Q}$.

By gradually increasing the applied magnetic field, the component of $\mathbf{M}$ parallel to $\mathbf{B}$ has a non-zero, increasing value in the conical phase, untill the saturation is reached and the system becomes completely polarized.

SKYRMION PHASE (A-PHASE) In a tiny pocket of the phase diagram, for temperatures just below T_C and finite magnetic field, a two-dimensional hexagonal lattice of Skyrmions oriented perpendicular to B is the ground state (see Fig. 1.3–B). The lattice constant of the Skyrmion lattice is given by $2\xi/\sqrt{3}$. The Skyrmion lattice decouples very efficiently from the atomic crystal lattice, such that the plane of the Skyrmion lattice orients perpendicular to B independently of the underlying atomic orientation. This phase is also referred to as "A-phase" for historical reasons, since this is the name it got when the magnetization texture of this phase was not properly understood. Before the discovery of the Skyrmion lattice it was believed that the A-phase was just a single helix with a spiral wave vector $\mathbf{Q}$ aligned perpendicular to the applied field.

To find such a minimal energy configuration, with the constraint that in the whole lattice

$$\mathbf{M}^2 = M_S^2 \tag{2.14}$$

we can use the method of Lagrange multipliers. Given the expression of the free energy

$$\mathcal{E} = \int d^3r \left[\alpha \mathbf{M}^2 + J(\nabla \mathbf{M})^2 + 2D\mathbf{M} \cdot (\nabla \times \mathbf{M}) - \mathbf{B} \cdot \mathbf{M} \right]. \tag{2.15}$$

we need to find a minimum of the functional

$$\mathcal{F} = \mathcal{E} - \int d^3r \, \lambda(\mathbf{r}) \left(\mathbf{M}(\mathbf{r})^2 - M_S^2 \right). \tag{2.16}$$

By calculating $\frac{\delta \mathcal{F}}{\delta \mathbf{M}} = 0$ we get (let us omit the $\mathbf{r}$ dependence of $\mathbf{M}$, $\mathbf{B}$ and λ):

$$\lambda \mathbf{M} = -J\Delta \mathbf{M} + 2D\nabla \times \mathbf{M} - \mathbf{B}. \tag{2.17}$$

To find λ multiply (dot product) both sides of (2.17) by $\mathbf{M}$ and use (2.14):

$$\lambda = -J\frac{\mathbf{M}\cdot\Delta\mathbf{M}}{M_S^2} + 2D\frac{\mathbf{M}\cdot\nabla\times\mathbf{M}}{M_S^2} - \frac{\mathbf{B}\cdot\mathbf{M}}{M_S^2}. \tag{2.18}$$

Plugging this expression of λ into Eq. (2.17) we obtain the equation to solve to find the minimum of the free energy:

$$\mathbf{B} + 2D\nabla\times\mathbf{M} = \left[J\left(\Delta - \frac{\mathbf{M}\cdot\Delta\mathbf{M}}{M_S^2}\right) + 2D\frac{\mathbf{M}\cdot\nabla\times\mathbf{M}}{M_S^2} + \frac{\mathbf{B}\cdot\mathbf{M}}{M_S^2}\right]\mathbf{M}. \tag{2.19}$$

Unfortunately, equation (2.19) is not analitically solvable. One can find good guesses to find local minima, or solve it numerically.

A SIMPLE SOLUTION A simple treatment to find the Skyrmion solution based on reference [29] exploiting the radial symmetry of Skyrmions is the following. First, let us work with a continuous field of fixed-magnitude spins $\mathbf{n} = S\mathbf{n}(\mathbf{r})$ (see also Appendix A) and further simplify using units in which $S = 1$. Let us, moreover, consider the case of a Skyrmion where the spins are parallel to the magnetic field at the periphery, and anti-parallel at the centre. A better choice of coordinates, given the symmetries, are polar coordinates

$$\mathbf{r} = (x, y, z) = (\rho\cos\varphi, \rho\sin\varphi, z_0),$$

where z_0 defines the xy-plane where the Skyrmion lies (the magnetic field is then in the z direction). In each point of space the spin can be described by the two spherical angles

$\Theta(\rho,\varphi)$ the angle from the positive z-axis,

$\Phi(\rho,\varphi)$ the angle taken counterclockwise from the positive x-axis on the xy-plane

by the vector

$$\mathbf{n}(\mathbf{r}) = (\sin\Theta(\rho,\varphi)\cos\Phi(\rho,\varphi), \sin\Theta(\rho,\varphi)\sin\Phi(\rho,\varphi), \cos\Theta(\rho,\varphi)). \tag{2.20}$$

Since the Skyrmion is a radially symmetric structure, we have

$$\begin{aligned}\Theta &= \Theta(\rho),\\ \Phi &= \varphi + \frac{\pi}{2}.\end{aligned} \tag{2.21}$$

Figure 2.3: Numerical solutions of Eq. (2.25) for different values of applied magnetic fields (here the number associated with each line is the ratio of B and the critical field B_C) showing the magnetization profile of a Skyrmion of size ξ. In the figure the x axis represents ρ in units of ξ (denoted D_0). Figure from [29]

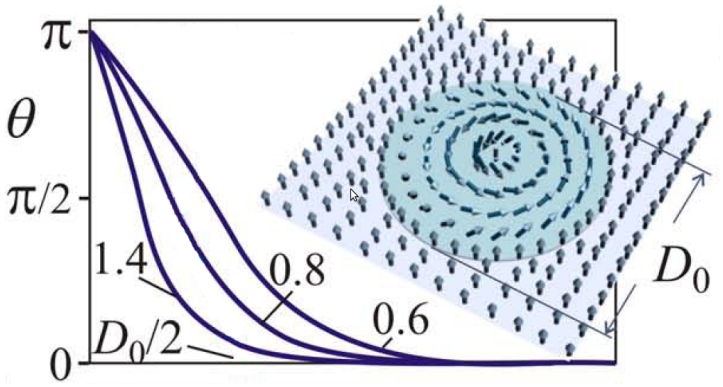

Dependencies (2.21) are a particular choice among different types of Skyrmions (cfr. Fig. 1.2). In these coordinates the free energy functional is

$$\mathcal{E} = \int \rho dz d\rho d\varphi \left[D\mathbf{n} \cdot \nabla \times \mathbf{n} + \frac{J}{2}(\nabla \mathbf{n})^2 + \mathbf{B} \cdot \mathbf{n} \right]. \tag{2.22}$$

Explicit calculation of terms in (2.22) using (2.20) and (2.21) gives

$$\mathcal{E} = \int \rho dz d\rho d\varphi \left[\frac{J}{2}\left(\Theta_\rho^2 + \frac{\sin^2\Theta}{\rho^2} \right) + D\left(\Theta_\rho + \frac{\sin\Theta\cos\Theta}{\rho} \right) - B\sin\Theta \right], \tag{2.23}$$

where subscript ρ denotes derivative w.r.t. ρ. From this expression of the energy $\mathcal{E} = \int \rho dz d\rho d\varphi\, \epsilon(\Theta, \Theta_\rho, \rho)$ we can find the differential equation governing $\Theta\rho$ in the Euler-Lagrange equation

$$\frac{\partial \epsilon}{\partial \Theta} - \frac{\partial}{\partial \rho}\frac{\partial \epsilon}{\partial \Theta_\rho} = 0, \tag{2.24}$$

and it is

$$J\left(\Theta_{\rho\rho} + \frac{1}{\rho}\Theta_\rho - \frac{\sin\Theta\cos\Theta}{\rho^2} \right) + 2D\frac{\sin^2\Theta}{\rho} - B\sin\Theta = 0\,. \tag{2.25}$$

Given the type of Skyrmion we are considering, the boundary conditions to this differential equation are

$$\begin{cases} \Theta(0) & = \pi; \\ \Theta(\infty) & = 0. \end{cases} \tag{2.26}$$

Eq. (2.25) was numerically solved in reference [29] and in Fig. 2.3 solutions $\Theta(\rho)$ are plotted for different values of the applied magnetic

field. The function $\Theta(\rho)$ is also called magnetization profile of the Skyrmion.

To conclude this section, it is important to mention that there are other mechanisms that contribute to lowering the energy functional and stabilize the Skyrmion phase that were not treated in this text. It has been shown in ref. [3] for example, that upon including Gaussian thermal fluctuations, the free energy of the Skyrmion phase becomes lower than the one of the conical phase, thereby favouring the Skyrmion lattice phase. Moreover, Butenko *et al.* have studied anisotropic terms in the free energy functional that could contribute to the global thermodynamic stability of the Skyrmion phase [30].

2.3 MICROSCOPIC MODELS AND COMPETING INTERACTIONS

We shall briefly discuss a microscopic model where helical ordering is obtained without the need of antisymmetric interactions between spins. The formations of spin spirals in such cases can be the result of competing ferromagnetic and anti-ferromagnetic interactions. Situations like these occur in nature, for example, in materials where the RKKY interaction is present, where the exchange constant between two interacting spins depends on their mutual distance (both in magnitude and sign).

Let us consider a simple case, which is a phenomenon that occurs in some real materials (e. g. Dysprosium) in the family of rare heart metals. These materials have a crystal structure such that the atoms lie in layers. In the case of Dysprosium, there is a magnetic phase in which the spins within the same layer align all parallel to each other, but at an angle with respect to spins in the neighbouring layer, say ϑ. For a simple argument, we only consider interactions between spins of nearest and next-nearest neighbouring layers. The interaction between two neighbouring layers (whose spins are at an angle ϑ between each other) can be described by the coupling constant J_1 and the interaction between two next-neighbouring layers (whose spins are at an angle 2ϑ between each other) by J_2. It is in all effects a 1D problem. The energy of this magnetic system is

$$\mathcal{E} = -J_1 \sum_{nn} \mathbf{S}_i \cdot \mathbf{S}_j - J_2 \sum_{nnn} \mathbf{S}_i \cdot \mathbf{S}_j, \tag{2.27}$$

and if all the spins have the same magnitude S, and there are in total N atoms, this expression can be simplified in

$$\mathcal{E} = -NS^2(J_1 \cos\vartheta + J_2 \cos 2\vartheta). \tag{2.28}$$

The energy is minimized for $\partial\mathcal{E}/\partial\vartheta = 0$, that is

$$\begin{aligned} J_1 \sin\vartheta + 2J_2 \sin 2\vartheta = J1 \sin\vartheta + 4J_2 \sin\vartheta \cos\vartheta = 0 \implies \\ \cos\vartheta = -\frac{J_1}{4J_2}. \end{aligned} \tag{2.29}$$

Figure 2.4: A triangular lattice. (Green) Red points are the (next-)nearest neighbours coupled through J_{FM} (J_{AFM}) to the blue point.

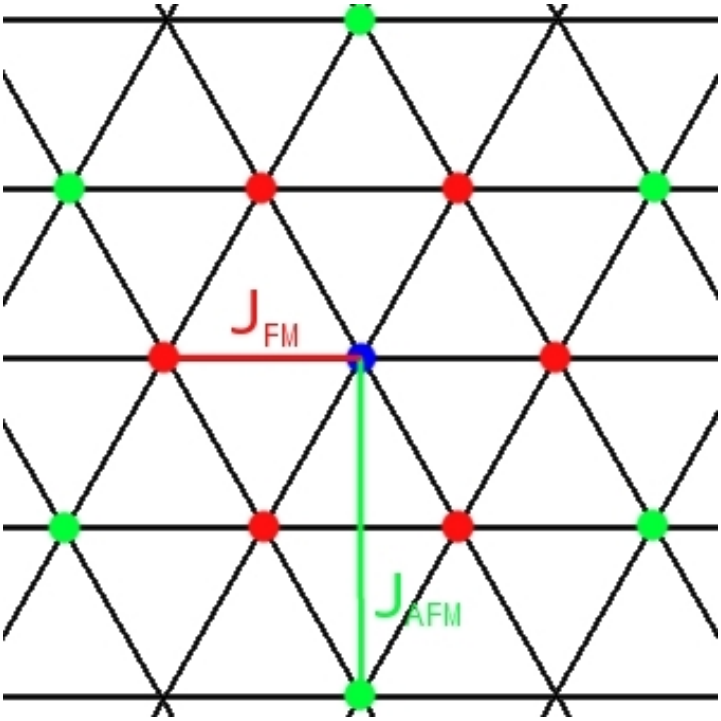

This last solution is a helical magnetic order. It is favoured over a ferromagnetic (or anti-ferromagnetic) ordering for $J_1 > 00$ (FM coupling, J_{FM}), $J_2 < 0$ (AFM coupling, J_{AFM}) and

$$\frac{|J_{AFM}|}{|J_{FM}|} > \frac{1}{4}. \tag{2.30}$$

There are no materials up to date that are known to host Skyrmions stabilized by competing FM-AFM interactions

A similar argument can be applied, at least theoretically, to the 2D problem where spins are displaced on a triangular lattice (see Fig. 2.4). Considering nn and nnn interactions with coupling constants J_{FM} and J_{AFM}, helical magnetism is possible if

$$\frac{|J_{AFM}|}{|J_{FM}|} > \frac{1}{3}. \tag{2.31}$$

In particular, a triple spiral state with the spirals wave vectors being equal to each other in magnitude and rotated by 120° angles , corresponding to a Skyrmion lattice, can be formed if

$$\frac{|J_{AFM}|}{|J_{FM}|} = \frac{1}{1+2\cos\left(\frac{2\pi}{\xi}\right)}, \tag{2.32}$$

where ξ is the lengthscale of such Skyrmions, and its range is dictated by (2.31). Inverting (2.32) we obtain the Skyrmion dimensions in this system:

$$\xi = \frac{2\pi}{\arccos\left(\frac{J_{FM}-J_{AFM}}{2J_AFM}\right)}. \tag{2.33}$$

3

SPIN TEXTURES MANIPULATION BY MEANS OF ELECTRICAL CURRENTS

In 2007 Peter Grünberg and Albert Fert were awarded the Nobel Prize in Physics for their independent findings, dating back to 1988, of the Giant Magneto-Resistance (GMR) effect [31, 32]. The ability to manipulate electrical currents by means of magnetism opened the way for an enormous step forward in data-storing applications. The opposite mechanism, i. e. the control of magnetic structures using (spin polarized) electrical currents, was proposed in 1996 by John Slonczewski and Luc Berger [33, 34]. This physical process is at the core of *Spintronics* and promises to be, in principle, even of more impact on applications, since in this way magnetic structures can be locally modified through the interaction with conduction electrons. The base mechanism is the spin-torque effect, which is the torque exerted by the conduction electrons spins on the magnetic textures in the material, causing it to move or change its state. The requirements for the spin-torque to be non-zero is that the magnetic structure varies in space and/or time. It has been extensively investigated, for example, that a force can be applied by a spin-polarized current onto magnetic domains, causing them to move. This is because a spin torque acts on the varying part of the magnetic configuration, i. e. the domain walls where spins are canted. Memory devices based on this concept have been proposed [14], however researchers have shown that current densities needed to start moving domain walls in real materials (i. e. affected by impurities and pinning effects) are too high ($j \sim 10^{11}\,\mathrm{A/m^2}$) to be appealing for competitive applications. Skyrmion magnetic structures, on the other hand, have been shown to couple very efficiently to spin-polarized electrical currents, thanks to the fact that they vary continuously and 'smoothly' in space. The threshold current densities needed to move them were measured (and theoretically estimated) to be five order of magnitude lower than the ones needed for domain walls motion.

In this chapter we shall start introducing a formalism to describe the interaction of conduction electrons and spin textures which is a direct consequence of the Berry phase accumulated by electrons in the adiabatic aproximation [35]. We shall continue discussing some of the measurable effects that are direct consequences of such interactions. Finally we will revise the Landau-Lifshitz-Gilbert equation and its most recent versions to describe the motions of spins in such structures, and the Thiele formalism to study the motion of the spin texture as a whole.

3.1 MOTION OF ELECTRONS THROUGH SKYRMIONS IN THE ADIABATIC APPROXIMATION

The adiabatic theorem, formulated in 1928 [36], states that a physical system remains in its instantaneous eigenstate if a given perturbation is acting on it slowly enough. We can help ourselves understanding the concept of an adiabatic process with a simple classical example: consider an oscillating pendulum attached to a moving support. If it moves fast (or at a comparable speed) with respect to the frequency of oscillations, the motion of the pendulum will be deeply affected, while if the support moves gradually and with a time-scale much longer than the period of the pendulum, the motion of the pendulum relative to its support remains unchanged, that is, the process is adiabatic. Applied to our conduction electron moving in a spin texture, this means that, in the adiabatic approximation, the exchange coupling J is much larger than the electron's kinetic energy, thus the conduction electron spin aligns to the local texture spin at a time-scale much shorter then the one of its motion. This is verified if the current density is low enough and if the Skyrmion size is much larger than the Fermi wavelength of the conduction electron. In this approximation, although its Hamiltonian is continuously changing, the wave function describing the conduction electron only gains a phase factor, called Berry phase. In the case of non-trivial spin textures like the Skyrmion, such a phase factor causes incredible (and measurable) physical effects, due to the emerging of effective electromagnetic fields directly related to it. In the following we shall derive such effective fields and describe some of their properties.

The motion of an electron is described by the Schrödinger equation:

$$\imath\hbar\frac{\partial\Psi}{\partial t} = \left[-\frac{\hbar^2}{2m}\Delta - J(\boldsymbol{\sigma}\cdot\mathbf{n})\right]\Psi, \tag{3.1}$$

where Ψ and m are the electron's spinor and mass, $\boldsymbol{\sigma}$ is the vector of Pauli matrices, J is the Heisenberg exchange coupling constant and $\mathbf{n}$ is the vector describing the spin texture (in units $S = 1$) of the Skyrmion. Since we are in the adiabatic approximation, we can write Ψ as the product of a spatial wave function and the texture spin vector:

$$\Psi = \chi\,|\mathbf{n}\rangle\,. \tag{3.2}$$

Substituting (3.2) in Eq. (3.1) we get

$$\imath\hbar\frac{\partial}{\partial t}\left(\chi\,|\mathbf{n}\rangle\right) = \left[-\frac{\hbar^2}{2m}\Delta - J(\boldsymbol{\sigma}\cdot\mathbf{n})\right]\chi\,|\mathbf{n}\rangle\,, \tag{3.3}$$

Multiply both sides of (3.3) by the bra $\langle\mathbf{n}|$:

$$\langle\mathbf{n}|\,\imath\hbar\frac{\partial}{\partial t}\left(\chi\,|\mathbf{n}\rangle\right) = \langle\mathbf{n}|\left[-\frac{\hbar^2}{2m}\Delta - J\right]\chi\,|\mathbf{n}\rangle\,, \tag{3.4}$$

where we have also used the fact that in the adiabatic approximation

$$J(\boldsymbol{\sigma}\cdot\mathbf{n})\,|\mathbf{n}\rangle = J\,|\mathbf{n}\rangle\,. \tag{3.5}$$

Performing all the derivatives we get

$$\imath\hbar\frac{\partial\chi}{\partial t} = \left[-\imath\hbar\,\langle\mathbf{n}|\,\partial_t\,|\mathbf{n}\rangle - J - \frac{\hbar^2}{2m}\Delta + \langle\mathbf{n}|\,\Delta\,|\mathbf{n}\rangle + 2\,\langle\mathbf{n}|\,\nabla\,|\mathbf{n}\rangle\cdot\nabla\right]\chi. \tag{3.6}$$

In Appendix B we show, using Bloch spherical representation, the following equalities:

$$\begin{aligned}
\langle\mathbf{n}|\,\partial_t\,|\mathbf{n}\rangle &= \frac{\imath}{2}(1-\cos\Theta)\dot{\Phi};\\
\langle\mathbf{n}|\,\nabla\,|\mathbf{n}\rangle &= \frac{\imath}{2}(1-\cos\Theta)\nabla\Phi;\\
\langle\mathbf{n}|\,\Delta\,|\mathbf{n}\rangle &= (\langle\mathbf{n}|\,\nabla\,|\mathbf{n}\rangle)^2 - \frac{1}{4}\partial_i n_j \partial_i n_j,
\end{aligned} \tag{3.7}$$

where $\Theta(\mathbf{r})$ and $\Phi(\mathbf{r})$ are the spherical angles describing the spin tecture. Plugging (3.7) back into Eq. (3.6) we obtain

$$\imath\hbar\frac{\partial\chi}{\partial t} = \left[\frac{\hbar}{2}(1-\cos\Theta)\dot{\Phi} + \frac{\left(\frac{\hbar}{\imath}\nabla + \frac{\hbar}{2}(1-\cos\Theta)\nabla\Phi\right)^2}{2m} - J + \frac{\hbar^2}{8m}\partial_i n_j \partial_i n_j\right]\chi \tag{3.8}$$

which is equivalent to the Schrödinger equation of an electron in an EM field if we define the effective 4-vector potential:

$$a_0 = \frac{\imath\hbar}{e}\,\langle\mathbf{n}|\,\partial_t\,|\mathbf{n}\rangle = -\frac{\hbar}{2e}(1-\cos\Theta)\dot{\Phi}; \tag{3.9}$$

$$\mathbf{a} = \frac{c\hbar}{\imath e}\,\langle\mathbf{n}|\,\nabla\,|\mathbf{n}\rangle = \frac{c\hbar}{2e}(1-\cos\Theta)\nabla\Phi\,, \tag{3.10}$$

where e is the electron charge and c the speed of light. The additional term $\propto \partial_i n_j \partial_i n_j$ is attributable to double exchange and it favours a ferromagnetic spin ordering.

The general form of the Hamiltonian describing the motion of an electron passing through a Skyrmion whose spins are described by $\mathbf{n}$ and with an applied EM field described by A_μ is finally

$$\mathcal{H} = \frac{\left(\frac{\hbar}{\imath}\nabla + \frac{e}{c}\boldsymbol{\alpha}\right)^2}{2m} - e\alpha_0 - J_{eff}\,, \tag{3.11}$$

where $\alpha_\mu = A_\mu + a_\mu$ is the total 4-vector potential and J_{eff} incorporates also the double exchange term.

3.2 EMERGING EM FIELDS AND TOPOLOGICAL EFFECTS

The effective 4-vector potential results in effective electro-magnetic fields felt by the conduction electrons even when there is no applied external field:

$$\mathbf{h} = \nabla\times\mathbf{a}\,; \tag{3.12}$$

$$\boldsymbol{e} = -\frac{1}{c}\dot{\mathbf{a}} - \nabla a_0\,. \tag{3.13}$$

Actually, these fields are always much larger than the external ones needed to stabilize the A-phase of Skyrmions. Furthermore, due to the particular dependence that they have on the spin texture, they have peculiar properties. We shall discuss them in the following.

Writing the effective magnetic field

$$h_i = \epsilon_{ijk}\partial_j a_k$$

using the expression for a_k in (3.10) leads

$$h_i = \epsilon_{ijk}\frac{\hbar c}{2e}\sin\Theta\partial_j\Theta\partial_k\Phi\,. \tag{3.14}$$

Exploiting the properties of the total anti-symmetric tensor ($\epsilon_{ijk} = -\epsilon_{ikj}$, etc...) we can write (3.14) like

$$h_i = \frac{1}{2}\epsilon_{ijk}\frac{\hbar c}{2e}\sin\Theta(\partial_j\Theta\partial_k\Phi - \partial_k\Theta\partial_j\Phi)\,. \tag{3.15}$$

In Appendix B we show that $\sin\Theta$ times the term in brackets in (3.15) is equal to the mixed product $(\mathbf{n}, \partial_j\mathbf{n}, \partial_k\mathbf{n}) = \mathbf{n}\cdot\partial_j\mathbf{n}\times\partial_k\mathbf{n}$, thus for example, for the z-component we have

$$\begin{aligned} h_z &= \frac{\hbar c}{2e}\mathbf{n}\cdot\partial_x\mathbf{n}\times\partial_y\mathbf{n} \\ &= \frac{hc}{e}\rho_Q \end{aligned} \tag{3.16}$$

where ρ_Q is the Skyrmion topological charge density as defined by the integrand of Eq. (1.1). A consequence of this is that the total flux of the efective magnetic field of a Skyrmion is

$$\phi = \int d^2x h_z = \frac{hc}{e}Q = Q\phi_0 = \pm\phi_0\,, \tag{3.17}$$

i. e. proportional to the topological charge, which is for a Skyrmion quantized and ± 1 most often. Furthermore it can be shown that for a moving Skyrmion with a drift velocity v_d, the emergent magnetic and electric fields are connected according to Faraday's law of induction, therefore the quantization of h_i is also transferred to e_i/v_d [23].

3.2.1 *Topological Hall Effect*

A direct consequence of the emerging electro-magnetic fields is that they contribute to the Hall resistivity in Hall measurements. Referring to a classical experimental setup as in Fig. 3.1, when a magnetic field is applied along the z-direction and and an electrical current flows in the x-direction, due to the Lorentz force that the electrons feel, a voltage is built in the y-direction. This voltage, the Hall voltage, can be measured and its dependence versus the magnetic field studied. The variable which is most often studied in experiments is the Hall

Figure 3.1: Hall effect experimental setup.

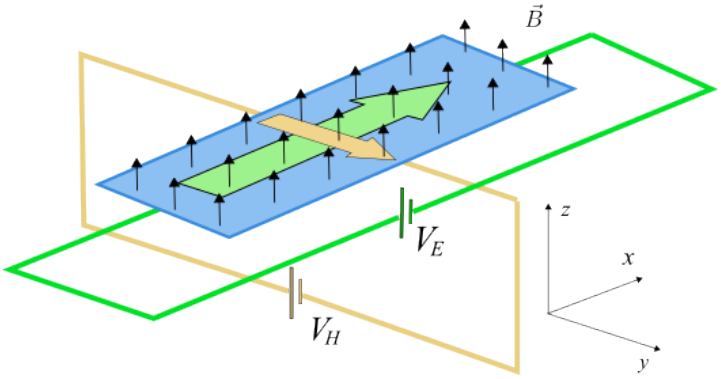

resistivity ρ_{xy}, defined as the Hall voltage divided by the applied electrical current. The subscript XY states the plane where the Hall and applied voltages are measured. For non-magnetic materials the Hall resistivity is linearly proportional to the applied magnetic field:

$$\rho_{xy} = R_H^0 B\,, \tag{3.18}$$

where R_H^0 is the Hall coefficient. For ferromagnetic materials, the net magnetization M increases the Hall resistivity proportionally to $\mu_0 M$ in what is called the Anomalous Hall Effect:

$$\rho_{xy} = R_H^0 B + R_H^{An} \mu_0 M\,. \tag{3.19}$$

Since the plane where the Skyrmion lattice (the A-phase) forms is perpendicular to the applied magnetic fields, in a Hall effect experiment the emerging magnetic field is parallel (or anti-parallel) to the applied magnetic field, and its contribution to the Hall resistivity was predicted to be [37, 38]

$$\Delta\rho_{xy} = \frac{p R_H^0}{2} h_z\,, \tag{3.20}$$

where p is the spin polarization of the current, which, e. g., for MnSi is ~ 0.1. Such a contribution was experimentally measured, ans was actually the first proof of the existence of such twirled spin texture phases [21]. Indeed, the emerging EM fields are not present in other phases, not in the helical phase, nor in the conical, making the detection of non-zero $\Delta\rho_{xy}$ a discriminant for the existence of Skyrmions, like shown in Fig. 3.2.

3.3 LLG EQUATION

We shall derive the equations of motion for the Skyrmion configuration $\mathbf{n}(\mathbf{r}, t)$, the Landau-Lifshitz-Gilbert (LLG) equation, via a variational principle.

Figure 3.2: Plot of the Skyrmion phase contribution to Hall resistance from the original work of Neubauer *et al* [21]. The top panel shows a plot of the Hall resistivity near the critical temperature, for applied fields corresponding to the A-phase. In the bottom panel the Skyrmion contribution to Hall resistivity is singled out, showing it is non-zero only when Skyrmion ordering is present.

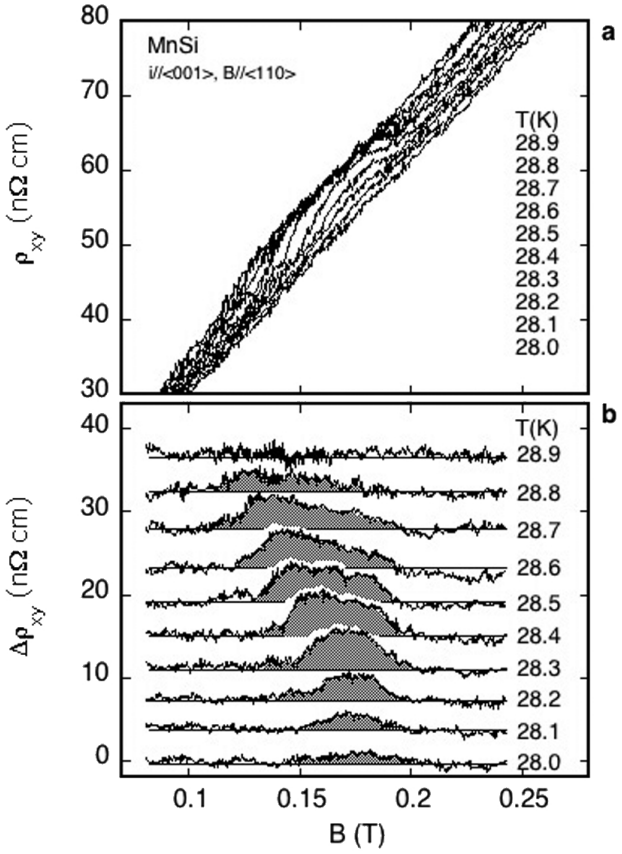

In the adiabatic motion, with the electron wave function being approximated by (3.2), the electron action can be written

$$\mathcal{S} = \int dt d^3r \left[\imath\hbar\chi^\dagger\dot{\chi} - \mathcal{H} \right] , \tag{3.21}$$

where the first term in the integrand is the Berry phase term for the spin action and the second term, the hamiltonian density, is the sum of the emerging fields hamiltonian $\mathcal{H}_0$ of Eq. (3.11), the interaction hamiltonian

$$\mathcal{H}_i = \rho a_0 - \frac{1}{c}\mathbf{j}\cdot\mathbf{a} \tag{3.22}$$

and the DM Hamiltonian

$$\mathcal{H}_{DM} = D\mathbf{n}\cdot(\nabla\times\mathbf{n}) , \tag{3.23}$$

where ρ and $\mathbf{j}$ are the electron density and current. The Berry phase term in Eq. (3.21) can be written

$$\mathcal{B} = \frac{1}{\nu}(\cos\Theta - 1)\dot{\Phi} , \tag{3.24}$$

where ν is the unit cell volume. If we express the electron density $\rho = -ex/\nu$ as the charge of the electron times the average number of electrons per site divided by the volume of the unit cell, we see that the term ρa_0 is proportional to the Berry phase term and the two can be summed in the spin action:

$$\rho a_0 = \frac{-ex}{\nu}\left(\frac{-\hbar}{2e}\right)(1-\cos\Theta)\dot{\Phi} = -\frac{x\hbar}{2\nu}(1-\cos\Theta)\dot{\Phi} . \tag{3.25}$$

We can thus re-write the spin action like

$$\mathcal{S} = \int dt d^3r \left\{ \gamma(\cos\Theta - 1)\dot{\Phi} + \frac{\hbar}{2e}\mathbf{j}\cdot[(1-\cos\Theta)\nabla\Phi] - \mathcal{H}' \right\} , \tag{3.26}$$

where we have defined $\gamma \equiv \hbar(S + x/2)/\nu$ and $\mathcal{H}' = \mathcal{H}_0 + \mathcal{H}_{DM}$, which from now on we will simply denote as $\mathcal{H}$. We note that the spin action does not trivially relate to the vector $\mathbf{n}$, since we only see the spherical angles defining $\mathbf{n}$ in this expression. Nevertheless, we shall find that the variation of the action relates in a nice way to the spin texture. Let us proceed in computing the variation of the action:

$$\begin{aligned} \delta S = \int dt d^3r \Big\{ & \gamma\left[-\sin\Theta\delta\Theta\dot{\Phi} + (\cos\Theta - 1)\delta\dot{\Phi}\right] \\ & + \frac{\hbar}{2e}\mathbf{j}\cdot[\sin\Theta\delta\Theta\nabla\Phi + (1-\cos\Theta)\delta(\nabla\Phi)] - \frac{\delta\mathcal{H}}{\delta\mathbf{n}}\delta\mathbf{n} \Big\} , \end{aligned} \tag{3.27}$$

integrating by parts the second and fourth terms we get

$$\begin{aligned} \delta S = \int dt d^3r \Big\{ & \gamma\sin\Theta\left(-\delta\Theta\dot{\Phi} + \dot{\Theta}\delta\Phi\right) \\ & + \frac{\hbar}{2e}\sin\Theta\mathbf{j}\cdot(\delta\Theta\nabla\Phi - \nabla\Theta\delta\Phi) - \frac{\delta\mathcal{H}}{\delta\mathbf{n}}\delta\mathbf{n} \Big\} . \end{aligned} \tag{3.28}$$

It is easy to show (cfr. Appendix B) that

$$\sin\Theta\left(-\delta\Theta\dot{\Phi}+\dot{\Theta}\delta\Phi\right)=\mathbf{n}\times\dot{\mathbf{n}}\cdot\delta\mathbf{n}$$

and

$$\sin\Theta\mathbf{j}\cdot\left(\delta\Theta\nabla\Phi-\nabla\Theta\delta\Phi\right)=\mathbf{n}\times(\nabla\cdot\mathbf{j})\mathbf{n}\cdot\delta\mathbf{n}$$

thus, by requiring $\delta\mathcal{S}/\delta\mathbf{n}=0$ we get the equations of motion for $\mathbf{n}$:

$$\mathbf{n}\times\left[\gamma\dot{\mathbf{n}}+\frac{\hbar}{2e}(\mathbf{j}\cdot\nabla)\mathbf{n}\right]=\frac{\delta\mathcal{H}}{\delta\mathbf{n}}\,. \tag{3.29}$$

We can further simplify this by multiplying (cross product) both sides of Eq. (3.29) and using $\mathbf{A}\times\mathbf{B}\times\mathbf{C}=\mathbf{B}(\mathbf{A}\cdot\mathbf{C})-\mathbf{C}(\mathbf{A}\cdot\mathbf{B})$ and the fact that $\mathbf{n}$ is a constant magnitude (=1) vector, therefore $\mathbf{n}\cdot\partial_\mu\mathbf{n}=0$. Finally we obtain the Landau-Lifshitz equation:

$$\dot{\mathbf{n}}=\gamma\mathbf{n}\times\left(-\frac{\delta\mathcal{H}}{\delta\mathbf{n}}\right)+\frac{\hbar\gamma}{2e}(\mathbf{j}\cdot\nabla)\mathbf{n}\,. \tag{3.30}$$

By defining the effective field $H^{eff}=-\frac{\delta\mathcal{H}}{\delta\mathbf{n}}$ and with the appropriate scaling of units, it can be rewritten:

$$\dot{\mathbf{n}}=\mathbf{n}\times H^{eff}+(\mathbf{j}\cdot\nabla)\mathbf{n}\,. \tag{3.31}$$

The term of Eq. (3.31) proportional to the current is called adiabatic spin-transfer torque.

The equation we have just derived is only valid in the total absence of damping and in a perfectly adiabatic process. For this equation to describe the minimal energy configuration in the totally polarized phase, we need to add a damping term, also called Gilbert damping (hence the name Gilbert-Landau-Lifshitz equation), which is defined by a positive constant α and is proportional to the cross product of the spin texture vector with its time derivative. This is because this damping torque should be always orthogonal to $\mathbf{n}$, since $\mathbf{n}$ is a vector of constant magnitude. Beside this damping term, a new non-adiabatic spin-transfer torque was introduced to account for small dissipative forces that break the conservation of spin in the spin transfer process. It is based on electron-spin relaxation phenomena and its coupling constant is usually β. The most general form of the LLG equation is then:

$$\dot{\mathbf{n}}=\mathbf{n}\times H^{eff}+(\mathbf{j}\cdot\nabla)\mathbf{n}+\alpha\mathbf{n}\times\partial_t\mathbf{n}-\beta\mathbf{n}\times(\mathbf{j}\cdot\nabla)\mathbf{n}\,. \tag{3.32}$$

This equation is widely and successfully used to solve spin dynamics in spintronics and related fields. We shall see, in the next section, how it simplifies if we assume a rigid drift of the spin texture as a whole:

$$\mathbf{n}(\mathbf{r},t)=\mathbf{n}(\mathbf{r}-\mathbf{R}(t))\,, \tag{3.33}$$

where $\mathbf{R}(t)$ describes the Center of Mass (CM) motion. This method, know as the Thiele method [39], will also allow us to calculate the forces acting on Skyrmions and estimate the drift velocity $\boldsymbol{v}_d$ in terms of the applied current and the LLG-equation parameters.

3.4 THIELE METHOD AND SKYRMION EQUATIONS OF MOTION

We start from the ansatz (3.33), justified by the phenomenological observation that after a current is applied, the non-collinear spin texture translates as a whole. We have then

$$\dot{\mathbf{n}} = -(\dot{\mathbf{R}} \cdot \nabla)\mathbf{n} \tag{3.34}$$

Assuming a rigid motion of the spin texture prevents this formalism to account for pinning forces, which have to be added in the future if needed for the case of study. Plugging (3.33) and (3.34) into the LLG equation we get:

$$-(\dot{\mathbf{R}} \cdot \nabla)\mathbf{n} = (\mathbf{j} \cdot \nabla)\mathbf{n} - \mathbf{n} \times \frac{\delta \mathcal{H}}{\delta \mathbf{n}} + \alpha \left[(\dot{\mathbf{R}} \cdot \nabla)\mathbf{n} \times \dot{\mathbf{n}}\right] - \beta \mathbf{n} \times (\dot{\mathbf{R}} \cdot \nabla)\mathbf{n}\,. \tag{3.35}$$

The idea of this method is to project the equation of motion onto the translational mode, which is the symmetry spontaneously broken when the Skyrmion lattice forms, on the plane perpendicular to the external magnetic field (the plane where Skyrmions lie). To do so , let us multiply equation (3.35) to the left by $(\mathbf{n}\times)$. Simplifying the multiple cross products, and using $\mathbf{j} = -\boldsymbol{v}^s$ (velocity of the spin polarized conduction electrons) in our scaled units, we get

$$(v_i^s - \dot{R}_i)\mathbf{n} \times \partial_i \mathbf{n} = -\left(n_i \frac{\delta \mathcal{H}}{\delta n_i}\right)\mathbf{n} + \frac{\delta \mathcal{H}}{\delta \mathbf{n}} - (\beta v_i^s - \alpha \dot{R}_i)\partial_i \mathbf{n}\,. \tag{3.36}$$

Multiply this (dot product) by $\partial_j \mathbf{n}$:

$$\frac{\delta \mathcal{H}}{\delta \mathbf{n}} \partial_j \mathbf{n} = (v_i^s - \dot{R}_i)(\mathbf{n}, \partial_i \mathbf{n}, \partial_j \mathbf{n}) + (\beta v_i^s - \alpha \dot{R}_i)\partial_i \mathbf{n} \partial_j \mathbf{n}\,. \tag{3.37}$$

Integrating Eq. (3.37) over a Skyrmion unit cell, we see that the LHS term becomes (minus) the derivative of the total energy of the Skyrmion with respect to the Skyrmion coordinates $(-\partial E/\partial R_j)$ since $\partial_j \mathbf{n} = -\partial \mathbf{n}/\partial R_j$. This is the force felt by the Skyrmion. Hence the two terms on the RHS can be analysed as the two direct effects of the spin-polarized current on the Skyrmion: the first term was defined by Thiele as the Gyromagnetic vector, since it transforms the spin current in a magnus force perpendicular to it. This term is clearly connected to the topological charge, in fact it is non-zero only for the A-phase; the second term is a dissipative term (dissipative tensor) and it describes drag forces. This final outcome, known as the Thiele equation, can be written as

$$\mathbf{F} = \mathbf{G} \times (\boldsymbol{v}^s - \dot{\mathbf{R}}) + \boldsymbol{\Gamma}(\beta \boldsymbol{v}^s - \alpha \dot{\mathbf{R}})\,, \tag{3.38}$$

where $\mathbf{G}$ and $\mathbf{\Gamma}$ are given by

$$G_i = \epsilon_{ijk} \int_{UC} d^2r(\mathbf{n}, \partial_i \mathbf{n}, \partial_j \mathbf{n}) , \tag{3.39}$$

$$\Gamma_{ij} = \int_{UC} d^2r \partial_i \mathbf{n} \partial_j \mathbf{n} . \tag{3.40}$$

Note that $\mathbf{F}$ vanishes (to lowest order in spin-orbit coupling) for a perfect Skyrmion lattice due to translational invariance. Further, if we consider an external magnetic field parallel to the z-direction and an in-plane excitation current, exploiting the symmetries of the system, the dissipation tensor has the following simple form

$$\mathbf{\Gamma} = \Gamma \begin{bmatrix} 1 & 0 & 0 \\ 0 & -1 & 0 \\ 0 & 0 & 0 \end{bmatrix} \tag{3.41}$$

and the gyrocoupling vector is just $\mathbf{G} = 4\pi Q \hat{z}$. Recasting the Thiele equation with these approximations we get a linear system of equations

$$4\pi Q \begin{bmatrix} 0 & -1 & 0 \\ 1 & 0 & 0 \\ 0 & 0 & 0 \end{bmatrix} (\boldsymbol{v}^s - \dot{\mathbf{R}}) + \Gamma \begin{bmatrix} 1 & 0 & 0 \\ 0 & 1 & 0 \\ 0 & 0 & 0 \end{bmatrix} (\beta \boldsymbol{v}^s - \alpha \dot{\mathbf{R}}) = 0 . \tag{3.42}$$

which is effectively two-dimensional (x and y components). Rearranging terms in (3.42) we obtain the equations of motion for the Skyrmion CM:

$$\begin{bmatrix} \alpha\Gamma & -4\pi Q \\ 4\pi Q & \alpha\Gamma \end{bmatrix} \dot{\mathbf{R}} = \begin{bmatrix} \beta\Gamma & -4\pi Q \\ 4\pi Q & \beta\Gamma \end{bmatrix} \boldsymbol{v}^s . \tag{3.43}$$

This system is always non-singular, and its solution is

$$\dot{\mathbf{R}} = \mathbf{V}_{Sk} = \frac{\beta}{\alpha} \boldsymbol{v}^s + \frac{\alpha - \beta}{\alpha^3 \left(\frac{\Gamma}{4\pi Q}\right)^2 + \alpha} \left(\boldsymbol{v}^s + \alpha \frac{\Gamma}{4\pi Q} \hat{z} \times \boldsymbol{v}^s \right) . \tag{3.44}$$

$\mathbf{V}_{Sk}$ is the drift velocity of the Skyrmions due to the spin-polarized current $\boldsymbol{v}^s$. It can be seen from its expression that, although it is the sum of 'drag' term and a 'magnus' term, this latter is much smaller or even zero since $\alpha \sim \beta$. Therefore the Skyrmion lattice is expected to translate almost parallel to the excitation current, at a small angle

$$\theta \approx (\alpha - \beta) \frac{\Gamma}{4\pi Q} . \tag{3.45}$$

The LLG equation and Thiele method are mostly applied for DM-stabilized skyrmions, since in this case the length scale of magnetic ordering is large enough to justify a continuous approximation of

the treatment. Such skyrmions typically have a radius of hundreds of lattice sizes, making the angles in between neighbouring spins indeed 'infinitesimal'. What happens then when the size of Skyrmions reduces to fifty, twenty, or even less than ten lattice constants? We have seen in the introduction and in Section 2.3 that, e. g. frustrated interactions can result in such nano-structures. Here the continuous treatment we just discussed clearly breaks down, or at least has some significant discrepancies. In the next chapter we shall cover this issue and attempt to find equations of motion for the Skyrmion in a microscopic model. Morover, the motion of quantum Skyrmions stabilized by frustrated exchange interactions on a triangular lattice will be studied through numerical simulations based on finite differences and the LLG equation.

4

QUANTUM-SKYRMIONS: ANALYTICAL AND NUMERICAL APPROACH

In the previous chapters of this thesis we have revised the state of the art of the theory regarding Skyrmions and motion of spin textures in general. Most of these theories, though, rely on the assumption that the structure described by spins vary smoothly in space and time, so one can use linear functions, differential operators and most importantly the adiabatic approximation, to describe energy functionals and equations of motion. These theories have explained (and predicted) extraordinarily well a vast range of experimental phenomena in their validity domains. When dealing with really nano-sized Skyrmions, on the other hand, we do need to develop a fully microscopic theory to describe their physics. In this chapter we shall discuss a model based on the Ferromagnetic Kondo Double Exchange. In this context we shall derive the equations of motion for the spin texture. We shall see that they do not reduce as nicely as in the continuum theory. As an approximation, we studied numerically the stability and motion of frustrated quantum skyrmion on a triangular lattice, with a method which is an 'hybrid' in between the discrete and continuous models, which includes non-adiabatic effects. In the last section we shall show the results obtained from these simulations.

4.1 EQUATIONS OF MOTION OF A SINGLE SPIN

Before going to the actual problem, let us review a simple, solvable case of the motion of a single spin. It is useful for we are going to attempt to simplify the actual e.o.m's with the same procedure. Consider the spin $\mathbf{S} = S\mathbf{n} = S(\sin\Theta\cos\Phi, \sin\Theta\sin\Phi, \cos\Theta)$ parametrized by the two spherical angles Θ and Φ and described by the Hamiltonian H. The action is

$$\mathcal{A} = \int dt \left[\hbar S \cos\Theta\, \dot{\Phi} - H(\Theta, \Phi)\right] . \tag{4.1}$$

Calculating variations of the action we find the eqations of motion:

$$\begin{cases} \frac{\delta\mathcal{A}}{\delta\Theta} = 0 \implies -\hbar S \sin\Theta\, \dot{\Phi} - \frac{\delta H}{\delta\Theta} = 0\,, \\ \frac{\delta\mathcal{A}}{\delta\Phi} = 0 \implies +\hbar S \sin\Theta\, \dot{\Theta} - \frac{\delta H}{\delta\Phi} = 0\,. \end{cases} \tag{4.2}$$

An orthonormal basis for spherical coordinated is the set of vectors

$$\begin{aligned}\hat{e}_1 &= (\cos\Theta\cos\Phi, \cos\Theta\sin\Phi, -\sin\Theta) = \frac{\partial \mathbf{n}}{\partial\Theta};\\ \hat{e}_2 &= (-\sin\Phi, \cos\Phi, 0) = \frac{1}{\sin\Theta}\frac{\partial \mathbf{n}}{\partial\Phi};\\ \hat{e}_3 &= (\sin\Theta\cos\Phi, \sin\Theta\sin\Phi, \cos\Theta) = \mathbf{n}\,.\end{aligned} \tag{4.3}$$

Multiplying Eq. (4.2)(I) by $\hat{e}_1$ and (4.2)(II) by $\hat{e}_2/\sin\Theta$ and summing the two equations we get

$$\hbar S(-\sin\Theta\,\dot{\Phi}\hat{e}_1 + \dot{\Theta}\hat{e}_2) = \frac{\delta H}{\delta\Theta}\hat{e}_1 + \frac{1}{\sin\Theta}\frac{\delta H}{\delta\Phi}\hat{e_2} = \frac{\delta H}{\delta \mathbf{n}}\,, \tag{4.4}$$

where the last equality follows from (4.3). Multiplying Eq. (4.4) by $(\mathbf{n}\times)$ (cross product) and using $\hat{e}_i \times \hat{e}_j = \epsilon_{ijk}\hat{e}_k$ we get

$$\begin{aligned}\hbar S(-\sin\Theta\,\dot{\Phi}\hat{e}_3 \times \hat{e}_1 + \dot{\Theta}\hat{e}_3 \times \hat{e}_2) &= \mathbf{n} \times \frac{\delta H}{\delta \mathbf{n}}\\ \implies \hbar S(\dot{\Theta}\hat{e}_1 + \sin\Theta\,\dot{\Phi}\hat{e}_2) &= \mathbf{n} \times \left(-\frac{\delta H}{\delta \mathbf{n}}\right)\\ \implies \hbar\dot{\mathbf{S}} &= \mathbf{S} \times \left(-\frac{\delta H}{\delta \mathbf{S}}\right),\end{aligned} \tag{4.5}$$

so we were able to obtain the equations describing the motion of $\mathbf{S}$ from equations for Θ and Φ.

4.2 EQUATIONS OF MOTION IN THE FERROMAGNETIC KONDO MODEL

Consider now the more complicated problem of a lattice of spins and the Ferromagnetic Kondo model. Our model consists of the double exchange term, which intrinsically includes the interplay between charge and spin, the Hund's rule coupling and the spin interactions (Exchange, DM):

$$H = -\sum_{nm} t_{nm} c_n^\dagger c_n - \frac{1}{2} J_H \sum_n \mathbf{S}_n \cdot c_n^\dagger \sigma c_n + H' \tag{4.6}$$

where t_{nm} is the transfer integral for the hopping from site m to site n, $c_n = (c_{n\uparrow}\ c_{n\downarrow})$ are the electron operators, J_H is the Hund's coupling constant and H' is the Hamiltonian for spin interactions. We shall call the other part of the hamiltonian the electron part H_e. H_e can be simplified in the approximation of an adiabatic process and large Hund's rule coupling. In this case we can write the electron operator as the product of a scalar, spin-independent operator and a spinor:

$$c_n = u_n d_n \tag{4.7}$$

where

$$u_n = u_n(\Theta_n, \Phi_n) = \begin{pmatrix} \cos\frac{\Theta_n}{2} \\ \sin\frac{\Theta_n}{2} e^{\imath\Phi_n} \end{pmatrix}, \tag{4.8}$$

and the Hund's rule coupling becomes

$$-\frac{1}{2}J_H \sum_n \mathbf{S}_n \cdot c_n^\dagger \boldsymbol{\sigma} c_n = -\frac{J_H S}{2} \sum_n d_n^\dagger u_n^\dagger (\boldsymbol{\sigma}\cdot\mathbf{n}) u_n d_n = \\ = -\frac{J_H S}{2} \sum_n d_n \dagger d_n . \tag{4.9}$$

We shall neglect this latter term, since it wont affect the significant part of the e.o.m's. The spin action in this case reads

$$\mathcal{A} = \int dt \left[\hbar S \sum_n \cos\Theta_n \dot{\Phi}_n + \imath\hbar \sum_n c_n^\dagger \dot{c}_n - H_e - H' \right]. \tag{4.10}$$

Making use of approximation (4.7) and notation(4.8) we can compute:

$$t_{nm} c_n^\dagger c_m = \tilde{t}_{nm} d_n^\dagger d_m , \tag{4.11}$$

where $\tilde{t}_{nm}$ is a complex effective hopping integral that can be written $t_{nm} u_n^\dagger u_m = \cos\frac{\Theta_{nm}}{2} e^{\imath\Phi_{nm}}$, with Θ_{nm} the angle between spins $\mathbf{S}_n$ and $\mathbf{S}_m$, the one defined by their dot product

$$\cos\Theta_{nm} = \cos\Theta_n \cos\Theta_m + \sin\Theta_n \sin\Theta_m \cos(\Phi_m - \Phi_n) ,$$

and Φ_{nm} a phase depending non-trivially from Φ_n and Φ_m:

$$\Phi_{nm} = \\ \arg(\tilde{t}_{nm}) = \arctan\left(\frac{\sin\frac{\Theta_n}{2}\sin\frac{\Theta_m}{2}\sin(\Phi_m - \Phi_n)}{\cos\frac{\Theta_n}{2}\cos\frac{\Theta_m}{2} + \sin\frac{\Theta_n}{2}\sin\frac{\Theta_m}{2}\cos(\Phi_m - \Phi_n)} \right). \tag{4.12}$$

Also useful in the derivation will be the term:

$$c_n^\dagger \dot{c_n} = d_n^\dagger u_n^\dagger (\dot{u}_n d_n + u_n \dot{d}_n) = d_n^\dagger \dot{d}_n + u_n^\dagger \dot{u}_n d_n^\dagger d_n \tag{4.13}$$

Substituting (4.11) and (4.13) into the action (4.10) we obtain

$$\mathcal{A} = \int dt \left[\hbar S \sum_n \cos\Theta_n \dot{\Phi}_n + \imath\hbar \sum_n (d_n^\dagger \dot{d}_n + u_n^\dagger \dot{u}_n d_n^\dagger d_n) \right. \\ \left. + \sum_{nm} \tilde{t}_{nm} d_n^\dagger d_m - H' \right]. \tag{4.14}$$

Equations of motion are then found like in (4.2) (we shall omit to write the integration over time, but this will be useful in some terms to be integrated by parts):

$$\text{(I)}\bullet\quad \frac{\delta H'}{\delta\Theta_n} = -\hbar S\sin\Theta_n\,\dot\Phi_n + \imath\hbar\frac{\delta}{\delta\Theta_n}(u_n^\dagger\dot u_n)d_n^\dagger d_n + \sum_m\left[t_{nm}\frac{\delta u_n^\dagger}{\delta\Theta_n}u_m d_n^\dagger d_m + t_{mn}u_m^\dagger\frac{\delta u_n}{\delta\Theta_n}d_m^\dagger d_n\right] \tag{4.15}$$

$$\text{(II)}\bullet\quad \frac{\delta H'}{\delta\Phi_n} = \hbar S\sin\Theta_n\,\dot\Theta_n + \imath\hbar\frac{\delta}{\delta\Phi_n}(u_n^\dagger\dot u_n)d_n^\dagger d_n + \sum_m\left[t_{nm}\frac{\delta u_n^\dagger}{\delta\Phi_n}u_m d_n^\dagger d_m + t_{mn}u_m^\dagger\frac{\delta u_n}{\delta\Phi_n}d_m^\dagger d_n\right] \tag{4.16}$$

★ *To get this equality this term is integrated by parts over time.*

The derivative terms in the equations above read:

$$\frac{\delta}{\delta\Theta_n}(u_n^\dagger\dot u_n) = \frac{\imath}{2}\sin\Theta_n\dot\Phi_n \tag{4.17}$$

$$\frac{\delta}{\delta\Phi_n}(u_n^\dagger\dot u_n) \overset{\bigstar}{=} -\frac{\imath}{2}\sin\Theta_n\dot\Theta_n \tag{4.18}$$

$$\begin{aligned}\frac{\delta u_n^\dagger}{\delta\Theta_n}u_m &= -\frac{1}{2}\sin\frac{\Theta_n}{2}\cos\frac{\Theta_m}{2} + \frac{1}{2}\cos\frac{\Theta_n}{2}\sin\frac{\Theta_m}{2}e^{\imath(\Phi_m-\Phi_n)}\\ &= \frac{1}{2}\sin\frac{\Theta_{nm}}{2}e^{\imath\xi_{nm}}\end{aligned} \tag{4.19}$$

where

$$\xi_{nm} = \arctan\left(\frac{\cos\frac{\Theta_n}{2}\sin\frac{\Theta_m}{2}\sin(\Phi_m-\Phi_n)}{\sin\frac{\Theta_n}{2}\cos\frac{\Theta_m}{2}+\cos\frac{\Theta_n}{2}\sin\frac{\Theta_m}{2}\cos(\Phi_m-\Phi_n)}\right) \tag{4.20}$$

$$\begin{aligned}u_m^\dagger\frac{\delta u_n}{\delta\Theta_n} &= -\frac{1}{2}\sin\frac{\Theta_n}{2}\cos\frac{\Theta_m}{2} + \frac{1}{2}\cos\frac{\Theta_n}{2}\sin\frac{\Theta_m}{2}e^{-\imath(\Phi_m-\Phi_n)}\\ &= \frac{1}{2}\sin\frac{\Theta_{nm}}{2}e^{-\imath\xi_{nm}}\end{aligned} \tag{4.21}$$

$$\frac{\delta u_n^\dagger}{\delta\Phi_n}u_m = -\imath\sin\frac{\Theta_n}{2}\cos\frac{\cos\Theta_m}{2}e^{\imath(\Phi_m-\Phi_n)} \tag{4.22}$$

$$u_m^\dagger\frac{\delta u_n}{\delta\Phi_n} = \imath\sin\frac{\Theta_n}{2}\cos\frac{\cos\Theta_m}{2}e^{-\imath(\Phi_m-\Phi_n)} \tag{4.23}$$

Using relations (4.17)–(4.23), after rearranging, equations (4.15) and (4.24) read

$$\text{(I)}\bullet\quad \frac{\hbar}{\gamma}\sin\Theta_n\,\dot\Phi_n = \frac{1}{2}\sum_m\left[t_{nm}\sin\frac{\Theta_{nm}}{2}e^{\imath\xi_{nm}}d_n^\dagger d_m + t_{mn}\sin\frac{\Theta_{nm}}{2}e^{-\imath\xi_{nm}}d_m^\dagger d_n\right] - \frac{\delta H'}{\delta\Theta_n} \tag{4.24}$$

$$\text{(II)}\bullet \quad -\hbar S\sin\Theta_n\dot{\Theta}_n = +\sum_m \Big[t_{nm}(-\imath\sin\frac{\Theta_n}{2}\cos\frac{\cos\Theta_m}{2}e^{\imath(\Phi_m-\Phi_n)})d_n^\dagger d_m + t_{mn}(\imath\sin\frac{\Theta_n}{2}\cos\frac{\cos\Theta_m}{2}e^{-\imath(\Phi_m-\Phi_n)})d_m^\dagger d_n\Big] - \frac{\delta H'}{\delta\Phi_n} \tag{4.25}$$

where we have defined

$$\gamma \equiv \left(S + \frac{d_n^\dagger d_n}{2}\right)^{-1} . \tag{4.26}$$

Symmetrizing on the dummy indices that appear in the sums: $f_{nm} = (f_{nm}+fmn)/2$ and expressing $d_n^\dagger d_m$ and $d_m^\dagger d_n$ by its symmetric and antisymmetric terms:

$$\begin{aligned} d_n^\dagger d_m &= \frac{1}{2}\left[(d_n^\dagger d_m + d_m^\dagger d_n) + (d_n^\dagger d_m - d_m^\dagger d_n)\right] \\ d_m^\dagger d_n &= \frac{1}{2}\left[(d_n^\dagger d_m + d_m^\dagger d_n) - (d_n^\dagger d_m - d_m^\dagger d_n)\right] , \end{aligned} \tag{4.27}$$

we get, after a bit of manipulation following the main steps of what we did in the previous section, and making the avergages at the end ($d_n^\dagger d_m \to \left\langle d_n^\dagger d_m\right\rangle$):

$$\begin{aligned} \frac{\hbar}{\gamma}\dot{\mathbf{n}_n} = \mathbf{n}_n \times \left(-\frac{\delta H'}{\delta \mathbf{n}_n}\right) &+ \frac{1}{4}\sum_m t_{nm}\sin\frac{\Theta_{nm}}{2}\left[\frac{\sin\xi_{nm}+\sin\chi_{nm}}{\sin\Theta_n}\hat{e}_1 + (\cos\xi_{nm}+\cos\chi_{nm})\hat{e}_2\right]\left\langle d_n^\dagger d_m + d_m^\dagger d_n\right\rangle \\ &+ \frac{1}{4\imath}\sum_m t_{nm}\sin\frac{\Theta_{nm}}{2}\left[\frac{\cos\xi_{nm}-\cos\chi_{nm}}{\sin\Theta_n}\hat{e}_1 + (\sin\chi_{nm}-\sin\xi_{nm})\hat{e}_2\right]\left\langle d_n^\dagger d_m - d_m^\dagger d_n\right\rangle \end{aligned} \tag{4.28}$$

where the other phase that appears in the square brackets is defined as

$$\chi_{nm} = \arctan\left(\frac{-\sin\frac{\Theta_n}{2}\cos\frac{\Theta_m}{2}\sin(\Phi_m-\Phi_n)}{\cos\frac{\Theta_n}{2}\sin\frac{\Theta_m}{2}+\sin\frac{\Theta_n}{2}\cos\frac{\Theta_m}{2}\cos(\Phi_m-\Phi_n)}\right) \tag{4.29}$$

or more simply

$$\begin{aligned} \frac{\hbar}{\gamma}\dot{\mathbf{n}}_j = \mathbf{n}_j \times \left(-\frac{\delta H'}{\delta \mathbf{n}_j}\right) &+ \sum_m \mathbf{F}(\Theta_j,\Theta_m,\Phi_j,\Phi_m)\left\langle d_j^\dagger d_m + d_m^\dagger d_j\right\rangle \\ &+ \sum_m \mathbf{G}(\Theta_j,\Theta_m,\Phi_j,\Phi_m)\left\langle d_j^\dagger d_m - d_m^\dagger d_j\right\rangle . \end{aligned} \tag{4.30}$$

Equation (4.28) is the equation of motion for the spins described by $\mathfrak{n}$. It contains, apart from the usual effective magnetic field, two main terms, both orthogonal (as it should be) to $\dot{\mathfrak{n}}$ since it is a precessing spin. We shall try to understand them by taking the limit of the almost ferromagnetic case (small Θs) and see what is their physical meaning (see next paragraph). We anticipate that the first term, proportional to $\left\langle d_n^\dagger d_m + d_m^\dagger d_n \right\rangle$ can be attributed to effective ferromagnetic coupling mediated by the conduction electrons, due to the double exchange in the Hamiltonian, while the second term, proportional to $\left\langle d_n^\dagger d_m - d_m^\dagger d_n \right\rangle$ is to be associated with the torque exerted from the spin-polarized conduction electrons to the spin texture. While it is intuitive to understand the meaning of Θ_{nm}, the phases ξ_{nm} and χ_{nm} are highly non-trivial, and deeper analysis on their behaviour with respect to Θs and Φs is needed.

FERROMAGNETIC LIMIT If we consider the case where spins are almost all parallel to each other (and to the z-axis), then $\sin\Theta \approx \Theta$ and $\cos\Theta \approx 1 - \Theta^2/2$. Let us rewrite the Hamiltonian H_e in this special case. The term $u_n^\dagger u_m$ becomes

$$u_n^\dagger u_m \approx \left(1 - \frac{\Theta_n^2}{8}\right)\left(1 - \frac{\Theta_m^2}{8}\right) + \frac{\Theta_n \Theta_m}{4} e^{\imath(\Phi_m - \Phi_n)} . \tag{4.31}$$

Notice that (let $S = 1$)

$$S^\pm = S^x \pm S^y = \sin\Theta e^{\imath\pm\Phi} \approx \Theta e^{\imath\pm\Phi} , \tag{4.32}$$

and

$$S_n^z S_m^z \approx \left(1 - \frac{\Theta_n^2}{8}\right)\left(1 - \frac{\Theta_m^2}{8}\right) \approx 1 - \frac{\Theta_n^2}{8} - \frac{\Theta_m^2}{8} . \tag{4.33}$$

Using (4.32) and (4.33), $u_n^\dagger u_m$ becomes

$$u_n^\dagger u_m \approx \frac{3}{4} + \frac{1}{4}(S_n^z S_m^z + S_m^+ S_n^-) , \tag{4.34}$$

and therefore

$$H_e \approx \frac{3}{4}\sum_{nm} t_{nm} d_n^\dagger d_n + \frac{1}{4}\sum_{nm} t_{nm}(S_n^z S_m^z + S_m^+ S_n^-) d_\dagger d_m \equiv H_0 + \dots . \tag{4.35}$$

Let us make this Hamiltonian symmetric and average out the fermionic degrees of freedom, similarly as we did previously:

$$\begin{aligned} H_e = H_0 &+ \frac{1}{8}\sum_{nm} t_{nm} \mathbf{S}_n \cdot \mathbf{S}_m \left\langle d_n^\dagger d_m + d_m^\dagger d_n \right\rangle \\ &+ \frac{1}{8\imath}\sum_{nm} t_{nm}(S_m^x S_n^y - S_m^y S_n^x) \left\langle d_n^\dagger d_m - d_m^\dagger d_n \right\rangle \end{aligned} \tag{4.36}$$

We see that if we define an effective Exchange coupling

$$J_{nm}^{eff} \equiv \frac{1}{4} t_{nm} \left\langle d_n^\dagger d_m + d_m^\dagger d_n \right\rangle , \tag{4.37}$$

the second term in this Hamiltonian is equivalent to the Heisenberg exchange interaction for the ferromagnetic coupling. To understand the last term, let us point out how the equations of motion for the electron density n_m at lattice point m look: (do not confuse this n with the one describing the spin texture)

$$\imath\hbar \dot{n}_m = \partial_t (d_m^\dagger d_m) = \partial_t \left[n_m, H \right] = \left[d_m^\dagger d_m, \sum_{nm} t_{nm} d_n^\dagger d_m \right] . \tag{4.38}$$

The only non vanishing commutators are

$$\frac{1}{\imath\hbar} \sum_l t_{ml} d_m^\dagger d_l - \frac{1}{\imath\hbar} \sum_l t_{lm} d_l^\dagger d_m = \sum_l I_{l\to m} - \sum_l I_{m\to l} \tag{4.39}$$

where we have introduced $I_{l\to m}$ as the micro-current from site l to site m. This is related to the current density expression. Let $\mathbf{x}_{m+\alpha/2}$ describe the midpoint coordinate of lattice points $\mathbf{x}$ and $\mathbf{x}+\alpha$, along the direction α, then the current density at point $\mathbf{x}_{m+\alpha/2}$ is given by

$$j^\alpha(\mathbf{x}+\alpha/2) = \frac{-e\left\langle \dot{n}_m \right\rangle}{a^2} = -\frac{e t_{nm}}{\imath\hbar a} \left\langle d_m^\dagger d_{m+\alpha} - d_{m+\alpha}^\dagger d_m \right\rangle . \tag{4.40}$$

So, noticing $(S_m^x S_n^y - S_m^y S_n^x) = \hat{z} \cdot \mathbf{S}_m \times \mathbf{S}_n$, the Hamiltonian can be written like

$$H = H_0 + \frac{1}{2} \sum_{nm} J_{nm}^{eff} \mathbf{S}_n \cdot \mathbf{S}_m - \frac{\hbar a^2}{4} \sum_m \sum_{\alpha=x,y} j^\alpha(\mathbf{x}+\alpha/2) \hat{z} \cdot (\mathbf{S}_m \times \mathbf{S}_n) \tag{4.41}$$

which shows clearly the spin-polarized nature of the term proportional to $\left\langle d_n^\dagger d_m - d_m^\dagger d_n \right\rangle$.

We have seen that analytical computation of equations for the motion of Skyrmions in the complete quantum model can be very complex, and one has to always make some approximations to achieve the goal. In the next chapter a numerical study for such a motion will be presented, and the obtained results compared with the predictions from the solvable models.

4.3 MOTION OF A TINY SKYRMION EXCITED BY SPIN-POLARIZED CURRENTS: NUMERICAL SIMULATION AND V-J RELATION

We have simulated the motion, due to an in-plane current excitation, of a small Skyrmion stabilized by frustrated exchange interactions on a triangular lattice (see Fig. 4.1). The size of the Skyrmion is given by the ratio of the competing interaction as in Eq. (2.33). The spin-torque coupling considered is the one present in the Landau-Lifshitz-Gilbert (LLG) equation.

Figure 4.1: A plot of the skyrmion configuration during the simulation. The color mapping indicates spin z-component going from -1 at the centre of the Skyrmion, to 1 at its perifery. The x and y components are plotted as arrows.

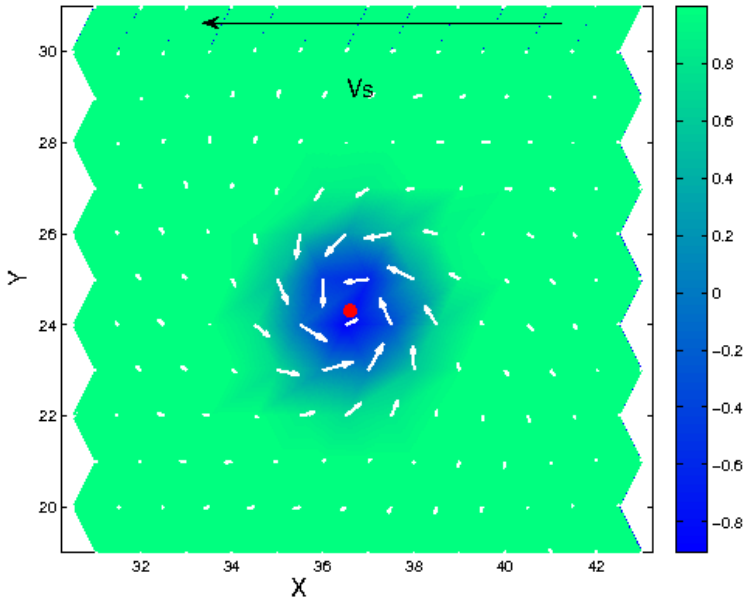

4.3.1 *Model and methods*

The frustration is given by the competition of ferromagnetic (J_{FM}) nearest-neighbour and anti-ferromagnetic (J_{AFM}) next nearest-neighbour interactions. The size of the Skyrmion is (in lattice constants):

$$\xi = \frac{2\pi}{\arccos\left(\frac{J_{FM}-J_{AFM}}{2J_{AFM}}\right)}. \tag{4.42}$$

In all of our simulations the skyrmion has a size of six lattice constants, given by $J_{AFM} = 1/2J_{FM}$.

We have numerically integrated the LLG equation at $T = 0$ using a fourth order Runge-Kutta algorithm (see Appendix C). The simulations were run for systems of 50x50, 150x150 and 250x250 sites of a triangular lattice, with spins described by the Hamiltonian

$$H = \sum_{nn} J_{FM}\mathbf{S}_i \cdot \mathbf{S}_j + \sum_{nn} J_{AFM}\mathbf{S}_i \cdot \mathbf{S}_j - B_z \sum_i S_{i,z} - K_z \sum_i S_{i,z}^2, \tag{4.43}$$

where K_z represents z-anisotropy. We also included non-adiabatic corrections (β) in the LLG equation:

$$\dot{\mathbf{S}} = -\mathbf{S} \times \mathbf{H}^{eff} + \alpha\mathbf{S} \times \dot{\mathbf{S}} + \frac{p}{2e}(\mathbf{j} \cdot \nabla)\mathbf{S} - \frac{p}{2e}\beta\mathbf{S} \times (\mathbf{j} \cdot \nabla)\mathbf{S}. \tag{4.44}$$

To evaluate this equation we need to express $\dot{\mathbf{S}}$ only in terms of $\mathbf{S}$ and derivatives. To do so, substitute for $\dot{\mathbf{S}}$ in the Gilbert damping

term, the expression given by the equation itself, use $\mathbf{A}\times\mathbf{B}\times\mathbf{C} = \mathbf{B}(\mathbf{A}\cdot\mathbf{C}) - \mathbf{C}(\mathbf{A}\cdot\mathbf{B})$ and the fact that $\mathbf{S}$ has unitary magnitude, so the product of it with time or space derivatives is zero. We get then the other form for the LLG equation:

$$\begin{aligned}\dot{\mathbf{S}} = &-\frac{1}{1+\alpha^2}\mathbf{S}\times\mathbf{H}^{eff} - \frac{\alpha}{1+\alpha^2}\mathbf{S}\times\mathbf{S}\times\mathbf{H}^{eff}\\ &+\frac{p}{2e}\frac{1+\alpha\beta}{1+\alpha^2}(\mathbf{j}\cdot\nabla)\mathbf{S} + \frac{p}{2e}\frac{\alpha-\beta}{1+\alpha^2}\mathbf{S}\times(\mathbf{j}\cdot\nabla)\mathbf{S}\,.\end{aligned} \tag{4.45}$$

The skyrmion solutions were found by minimizing the magnetic energy with a Monte Carlo method and then by further relaxing the spin texture by integrating the LLG equation for $j = 0$. We used a value of $\alpha = 0.03$, which is the typical value for ferromagnetic metal, and $\beta = \alpha$. In the natural units of the simulation, $J_{FM} = 1 = 2J_{AFM}$ and $B = 0.4$. After good convergence of the spin configuration was achieved, checked by energy calculations, we switched on a steady electric current density $\mathbf{j} = j_x\hat{x}$, spin polarized and with polarization $p = 0.2$, and then studied the dynamics of the spin texture. The units of our simulation are, for time $\tau = \hbar/J_{FM}$ and for current $\kappa = 2eMJ_{FM}/a^2\hbar$. Considering a typical lattice size $a = 5\text{Å}$ and magnitude of local magnetic moment $M = 1$, the values of τ and κ are $\tau \simeq 6.5\cdot10^{-13}$ s and $\kappa \simeq 2\cdot10^{-12}$ A/m^2, respectively. The unit of velocity is then $\mu \simeq 7.8\cdot10^{2}$ ms^{-1}.

4.3.2 *Results and conclusions*

The center-of-mass motion for several values of the applied external current are shown in figure 4.2. From this figure it can be seen that, for all values of the current, the motion of the skyrmions starts off at a large angle with respect to the conduction electrons velocity (cfr. V_s Fig. 4.1). Successively they reach a steady state angle, corresponding to steady values of x and y components of velocity. This behaviour is evident from the plot in Fig. 4.3, where it can also be noticed that there are some oscillations even in the steady state phase of the motion, with amplitudes proportional to the applied current and frequencies ranging in the GHz range. These oscillation can be the result of rotation of the skyrmion together with translation, while the varying of the amplitudes can be an effect of instability versus the applied electrical current. Indeed we found that for values of the current already from $\sim 1.5\cdot10^{10}$ Am^{-2} these oscillation diverge, indicating a destruction of the skyrmion, or in other words a transition to a more favourable magnetic state. This can be clearly seen from a plot of the total magnetic energy with respect to the the ferromagnetic state (shown in Fig. 4.4–A) and of the Skyrmion topological charge (Fig. 4.4–B). To better understand this behaviour of the Skyrmion, a deeper investigation is needed. For example, exploring different values of the parameters (like applied magnetic field, anisotropy con-

Figure 4.2: Numerical solutions of the center of mass motion of a single Skyrmion for different magnitudes of the applied current on the x-direction.

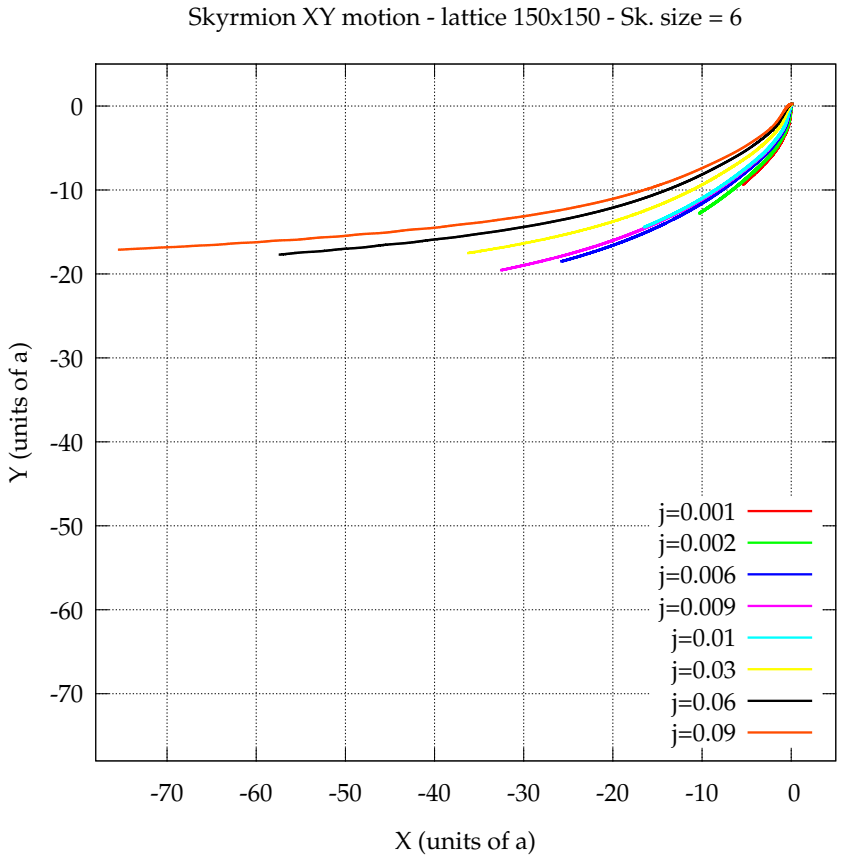

Figure 4.3: Drift angle of the Skyrmion centre of mass plotted versus time. The angle has a maximum at the beginning of the motion while it reaches a steady state value for long integration time, where some oscillations are also present. These oscillation might be the effect of the rotation of the Skyrmion or of instabilities due to the metastable nature of the spin state.

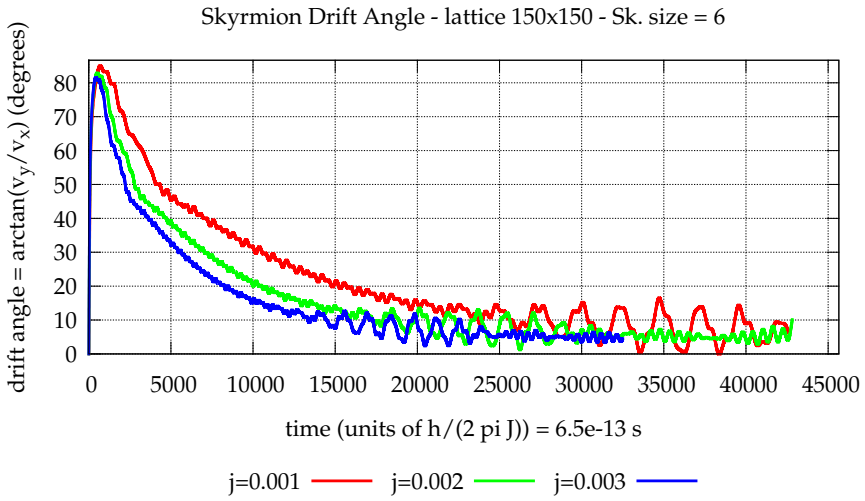

stant and J_{AFM}/J_{FM}), to put ourself in different points of the phase diagram. These fluctuations can in fact be the result of a state too close to a phase transition point, thus resulting in instabilities. Further investigation is also required about the rotational behaviour of the motion, where we could introduce a quantization of the total angular momentum proper of a system of nanometres size dominated by quantum physics. Given our parameters, we have seen however the tendency to reach a steady average drift velocity v_d. A plot of the parallel component to the current is shown in Fig. 4.5. As expected from simulations and experiments on bigger types of Skyrmions (stabilized by antisymmetric interactions) and from the Thiele equation, the drift velocity is linearly proportional to the applied current density, and the numerical values are actually comparable to the ones of the universal current-velocity relation found by Iwasaki and coworkers [40] for Skyrmions (lattice phase) 50 lattice constants big.

A major improvement of this simulation is to be searched in the solution of the problem stated in the previous section 4.2. Of particular relevance would be the understanding of the last term in Eq. (4.28), to obtain a form of the spin-torque coupling coming entirely from a microscopic model.

Figure 4.4: Figures showing the instability of the small single Skyrmion versus the applied electric current. Panel A shows the total mgnetic energy with respect to the ferromagnetic phase, while Panel B a plot of the Skyrmion topological charge w.r.t. time. There occurs a phase transition to a state close to FM in energy and with zero topological charge for bigger values of currents.

A

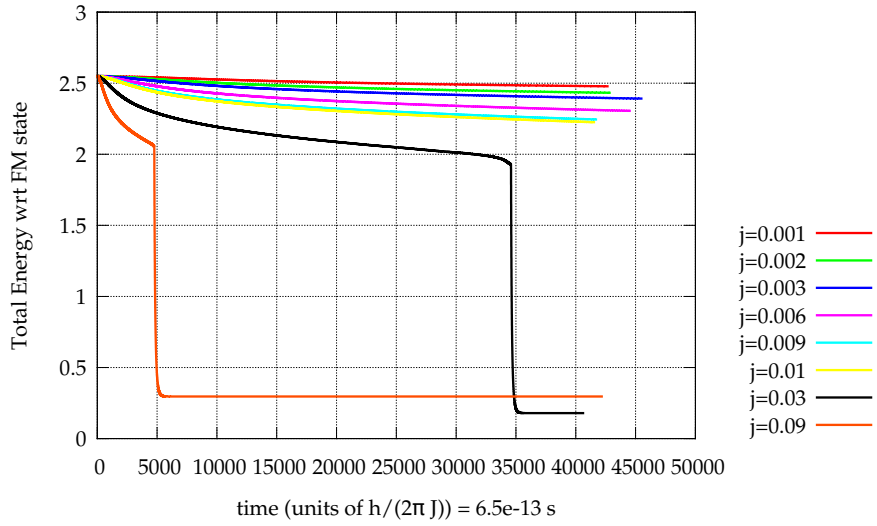

B

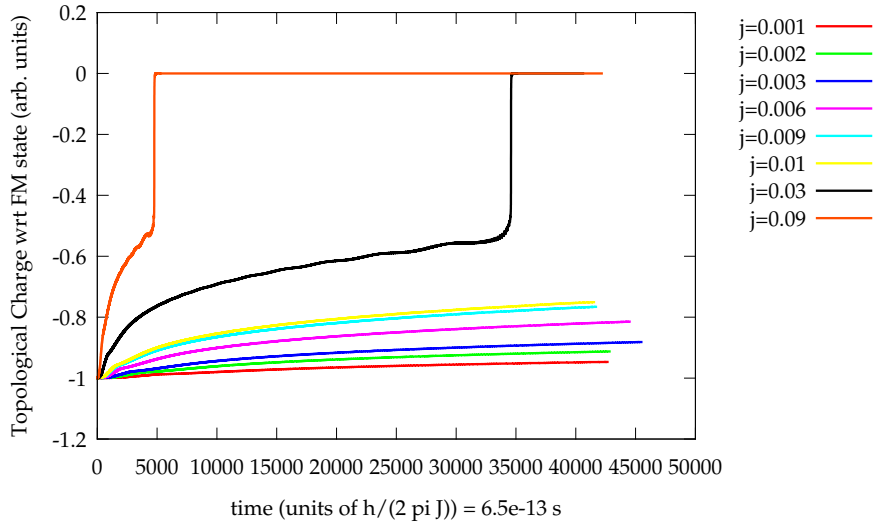

Figure 4.5: $v - j$ relation for a small, single Skyrmion showing a linear dependence at low currents.

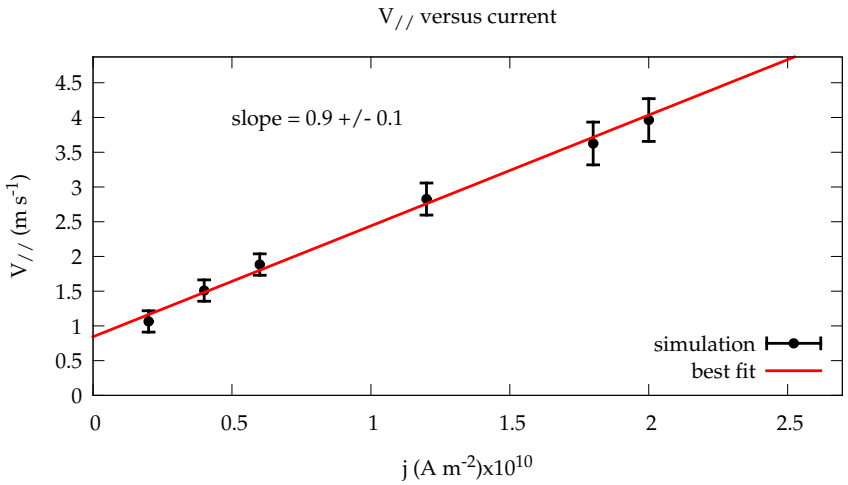

To conclude, we have attempted at deriving equations for the motion of Skyrmions excited by means of spin-polarized currents excitation, where more research is needed in to unfold the interpretation of functions **F** and **G** of Eq. (4.30) in order to decouple the persistent spin-current terms coming from the non-zero Berry phase from the applied currents of which we want to study the spin-torque effect. For the sake of approaching a complete microscopic understanding of Skyrmion dynamics, we have also numerically simulated the motion of a tiny Skyrmion stabilized by frustrated exchange interactions. By using a discretized version of the classical LLG equation, we have found that also for such small Skyrmions there is a linear dependence between their drift velocity and the applied electric current. We have seen, however, unusual behaviours related to initial phases of the motion and rotational patterns in the steady state. Further development of this research will include the quantization of such rotations and the systematic study of the Skyrmion drifting motion for a wider range of parameters of the Hamiltonian.

APPENDIX

A

THE TOPOLOGICAL CHARGE

A.1 GEOMETRICAL MEANING

The spin direction $\mathbf{n}(x, y)$ subject to the constraint

$$\sum_{\alpha} n_{\alpha}(x, y) = 1 \tag{A.1}$$

can be described in terms of the two spherical angles $\Theta(x, y)$ and $\Phi(x, y)$. Thus we can write $\mathbf{n}(\Theta(x, y), \Phi(x, y))$, and the spatial derivatives become

$$\begin{aligned} \partial_x \mathbf{n} &= \partial_\Theta \mathbf{n}\, \partial_x \Theta + \partial_\Phi \mathbf{n}\, \partial_x \Phi, \\ \partial_y \mathbf{n} &= \partial_\Theta \mathbf{n}\, \partial_y \Theta + \partial_\Phi \mathbf{n}\, \partial_y \Phi. \end{aligned} \tag{A.2}$$

The cross product between these partial derivatives is thus transformed as

$$\partial_x \mathbf{n} \times \partial_y \mathbf{n} = (\partial_\Theta \mathbf{n} \times \partial_\Phi \mathbf{n})\,(\partial_x \Theta\, \partial_y \Phi - \partial_x \Phi\, \partial_y \Theta) \tag{A.3}$$

The last term in brackets in Eq. (A.3) is the inverse Jacobian

$$(|J|^{-1}) = \left[\det \begin{pmatrix} \partial_\Phi x & \partial_\Theta x \\ \partial_\Phi y & \partial_\Theta y \end{pmatrix} \right]^{-1}$$

of the transformation we are considering:

$$\begin{aligned} x &= \sin(\Theta)\cos(\Phi), \\ y &= \sin(\Theta)\sin(\Phi). \end{aligned} \tag{A.4}$$

Expressing the topological charge in spherical coordinates we get

$$\begin{aligned} Q &= \frac{1}{4\pi} \iint d^2x\, \mathbf{n} \cdot (\partial_x \mathbf{n} \times \partial_y \mathbf{n}) \\ &\overset{(A.3)}{=} \frac{1}{4\pi} \iint |J|\, d\Theta d\Phi\, \mathbf{n} \cdot (\partial_\Theta \mathbf{n} \times \partial_\Phi \mathbf{n})\, |J|^{-1} \\ &= \frac{1}{4\pi} \iint d\Theta d\Phi\, \mathbf{n} \cdot (\partial_\Theta \mathbf{n} \times \partial_\Phi \mathbf{n})\,. \end{aligned} \tag{A.5}$$

Since we have the constraint (A.1), the integrand in the last expression is the solid angle element

$$d\Omega = d\Theta\, d\Phi \mathbf{n} \cdot \partial_\Theta \mathbf{n} \times \partial_\Phi \mathbf{n}, \tag{A.6}$$

thus we see that the topological charge is

$$Q = \frac{1}{4\pi} \iint d\Omega, \tag{A.7}$$

i. e. the number of times $\mathbf{n}$ wraps the unit sphere as we span the coordinate space $\mathbb{R}^2$.

A.2 EXPLICIT CALCULATION

Using the radial symmetry of the skyrmion we can write

$$\Theta = \Theta(\rho), \tag{A.8}$$
$$\Phi = \Phi(\varphi) = m\varphi + \gamma, \tag{A.9}$$

where we have introduced the vorticity m, the helicity γ (see Fig. 1.2) and the polar coordinates $\mathbf{r} = (x, y) = (\rho\cos(\varphi), \rho\sin(\varphi))$. Thus the spin direction vector field can be written

$$\mathbf{n}(\mathbf{r}) = (\sin\Theta(\rho)\cos\Phi(\varphi), \sin\Theta(\rho)\sin\Phi(\varphi), \cos\Theta(\rho)). \tag{A.10}$$

Using this in Eq. (A.5) we get

$$\begin{aligned} Q &= \frac{1}{4\pi}\int_0^\infty d\rho \int_0^{2\pi} \frac{d\Theta(\rho)}{d\rho}\frac{d\Phi(\varphi)}{d\varphi}\sin\Theta(\rho) \\ &= [\cos\Theta(\rho)]_{\rho=0}^{\rho=\infty}\,[\Phi(\varphi)]_{\varphi=0}^{\varphi=2\pi}, \end{aligned} \tag{A.11}$$

If we consider the case of a skyrmion in a FM background where spins point in the positive z direction (and so $\Theta(\rho=\infty)=0$), then at the center of the skyrmion the spin points down ($\Theta(\rho=0)=\pi$), thus $[\cos\Theta(\rho)]_{\rho=0}^{\rho=\infty} = 2$. The vorticity is defined as $m = {}^{[\Phi(\varphi)]_{\varphi=0}^{\varphi=2\pi}}/_{2\pi} = \pm 1$, hence we have that

$$Q = m = \pm 1. \tag{A.12}$$

For DM stabilized skyrmions, the lowest energy configuration has $m = +1$ and $\gamma = \pm\pi/2$, where the sign of γ is determined by the vector $\mathbf{D}$, in turn determined by the crystal symmetries. For skyrmions forming through four-spin exchange or frustrated exchange interactions, all cases ($m = \pm 1$, $\gamma = 0, \pm\pi/2, \pi$) are degenerate.

B

SPIN STATE AND THE BLOCH SPHERICAL REPRESENTATION

The spin state can be described as a superposition of $|\uparrow\rangle$ and $|\downarrow\rangle$ in the Bloch representation as

$$|\mathbf{n}\rangle = \cos\frac{\Theta}{2}|\uparrow\rangle + \sin\frac{\Theta}{2}e^{\imath\Phi}|\downarrow\rangle\,, \tag{B.1}$$

where $\Theta(\mathbf{r})$ and $\Phi(\mathbf{r})$ describe the spin orientation in spherical coordinates. Using (B.1) we can explicitly compute some of the numerical quantities needed for the derivations in the main text of this thesis.

B.1 COMPUTATION OF $\langle\mathbf{n}|\,\partial_t\,|\mathbf{n}\rangle$, $\langle\mathbf{n}|\,\nabla\,|\mathbf{n}\rangle$ AND $\langle\mathbf{n}|\,\Delta\,|\mathbf{n}\rangle$

This is a straightforward computation, so we shall perform it for the first term and only state the result for the other two, found in a similar way:

$$\begin{aligned}\langle\mathbf{n}|\,\partial_t\,|\mathbf{n}\rangle &= \begin{pmatrix}\cos\frac{\Theta}{2} & \sin\frac{\Theta}{2}e^{-\imath\Phi}\end{pmatrix}\partial_t\begin{pmatrix}\cos\frac{\Theta}{2}\\ \sin\frac{\Theta}{2}e^{\imath\Phi}\end{pmatrix}\\ &= \begin{pmatrix}\cos\frac{\Theta}{2} & \sin\frac{\Theta}{2}e^{-\imath\Phi}\end{pmatrix}\begin{pmatrix}-\frac{\dot\Theta}{2}\sin\frac{\Theta}{2}\\ \left(\frac{\dot\Theta}{2}\cos\frac{\Theta}{2}+\imath\dot\Phi\sin\frac{\Theta}{2}\right)e^{\imath\Phi}\end{pmatrix}\\ &= \imath\left(\sin\frac{\Theta}{2}\right)^2\dot\Phi = \frac{\imath}{2}(1-\cos\Theta)\dot\Phi\,.\end{aligned} \tag{B.2}$$

In a similar fashion we obtain the rest of relations (3.7).

B.2 SPIN VECTOR AND MIXED PRODUCTS

Let us prove, by explicit calculation of the RHS, the equality

$$\sin\Theta(\partial_j\Theta\partial_k\Phi - \partial_k\Theta\partial_j\Phi) = \mathbf{n}\cdot\partial_j\mathbf{n}\times\partial_k\mathbf{n}\,. \tag{B.3}$$

Expressing $\mathbf{n}$ in its Cartesian coordinates:

$$\mathbf{n} = (\sin\Theta\cos\Phi, \sin\Theta\sin\Phi, \cos\Theta) \tag{B.4}$$

we have

$$\partial_j\mathbf{n} = \begin{pmatrix}\cos\Theta\cos\Phi\partial_j\Theta - \sin\Theta\sin\Phi\partial_j\Phi\\ \cos\Theta\sin\Phi\partial_j\Theta + \sin\Theta\cos\Phi\partial_j\Phi\\ -\sin\Theta\partial_j\Theta\end{pmatrix}\,. \tag{B.5}$$

Then, we can proceed in computing the cross product:

$$\partial_j \mathbf{n} \times \partial_k \mathbf{n} = \begin{vmatrix} \hat{x} & \hat{y} & \hat{z} \\ \partial_j n_x & \partial_j n_y & \partial_j n_z \\ \partial_k n_x & \partial_k n_y & \partial_k n_z \end{vmatrix} : \tag{B.6}$$

$$\begin{aligned} \underline{\text{X-component}} &= -\sin\Theta\partial_k\Theta(\cos\Theta\sin\Phi\partial_j\Theta + \sin\Theta\cos\Phi\partial_j\Phi) \\ &\quad + \sin\Theta\partial_j\Theta(\cos\Theta\sin\Phi\partial_k\Theta + \sin\Theta\cos\Phi\partial_k\Phi) \\ \underline{\text{Y-component}} &= +\sin\Theta\partial_k\Theta(\cos\Theta\cos\Phi\partial_j\Theta - \sin\Theta\sin\Phi\partial_j\Phi) \\ &\quad - \sin\Theta\partial_j\Theta(\cos\Theta\cos\Phi\partial_k\Theta - \sin\Theta\sin\Phi\partial_k\Phi) \\ \underline{\text{Z-component}} &= \\ (\cos\Theta\cos\Phi\partial_j\Theta - \sin\Theta\sin\Phi\partial_j\Phi)&(\cos\Theta\sin\Phi\partial_k\Theta + \sin\Theta\cos\Phi\partial_k\Phi) \\ -(\cos\Theta\cos\Phi\partial_k\Theta - \sin\Theta\sin\Phi\partial_k\Phi)&(\cos\Theta\sin\Phi\partial_j\Theta + \sin\Theta\cos\Phi\partial_j\Phi) \end{aligned}$$

Finally, multiplying (dot product) this with $\mathbf{n}$:

$$\begin{aligned} \mathbf{n}\cdot\partial_j\mathbf{n}\times\partial_k\mathbf{n} &= -\sin^3\Theta\partial_k\Theta\partial_j\Phi + \sin^3\Theta\partial_j\Theta\partial_k\Phi - \sin\Theta\cos^2\Theta\partial_k\Theta\partial_j\Phi \\ &\quad + \sin\Theta\cos^2\Theta\partial_j\Theta\partial_k\Phi = \sin\Theta\partial_j\Theta\partial_k\Phi\left(\cos^2\Theta + \sin^2\Theta\right) \\ &\quad - \sin\Theta\partial_k\Theta\partial_j\Phi\left(\cos^2\Theta + \sin^2\Theta\right) = \sin\Theta(\partial_j\Theta\partial_k\Phi - \partial_k\Theta\partial_j\Phi) \end{aligned}$$

we get the equality (B.3). It can be similarly shown that

$$\sin\Theta\left(-\delta\Theta\dot{\Phi} + \dot{\Theta}\delta\Phi\right) = \mathbf{n}\times\dot{\mathbf{n}}\cdot\delta\mathbf{n} \tag{B.7}$$

and

$$\sin\Theta\mathbf{j}\cdot(\delta\Theta\nabla\Phi - \nabla\Theta\delta\Phi) = \mathbf{n}\times(\nabla\cdot\mathbf{j})\mathbf{n}\cdot\delta\mathbf{n}\,. \tag{B.8}$$

C

FOURTH ORDER RUNGE-KUTTA METHOD

The family of Runge-Kutta algorithms are amongst the most robust and consistent methods used in the numerical integration of differential equations. The problem to solve is of the type $\dot{x} = f(x,t), x(0) = x_0$. At a particular order N this method finds the approximated value of the function at time $t + dt$, by knowing the function and its derivative at time t, as a weighted average of N points interpolated in the time interval dt with different estimations of the gradient of x. In the fourth order case, the most used of these methods for the good balance of accuracy and computing costs, the algorithm (RK4) reads:

$$\begin{aligned} x(t+dt) &= x(t) + \frac{dt}{6}(k_1 + 2k_2 + 2k_3 + k_4) \\ k_1 &= f(t, y(t)) \\ k_2 &= f(t + \frac{dt}{2}, x(t) + \frac{dt}{2}k_1) \\ k_3 &= f(t + \frac{dt}{2}, x(t) + \frac{dt}{2}k_2) \\ k_4 &= f(t + dt, x(t) + dtk_3) \end{aligned} \tag{C.1}$$

More weight is given to the increments estimated by the slopes at middle interval points. The weights are such that, if f does not depend on x (normal integral), then this algorithm corresponds to Simpson's method for integrals. The RK4 method is a fourth-order method, meaning that the local truncation error is of the order of $O(dt^5)$, while the total accumulated error is order $O(dt^4)$.

In our simulation we have such equations for each of the three components of spin, and f is a vector given by the LLG equation. An extract of the code is shown in Listing C.1.

Listing C.1: RK4 algorithm example in matlab.

```
% INPUT PARAMETERS
% dt        = integration step
% Sx,Sy,Sz  = value of spins at time t
% a         = Gilbert damping
% b         = non-adiabatic effects
% J1,J2     = nn and nnn Exchange constants (>0)
% Hx,Hy,Hz  = magnetic field
% Kz        = Z-anisotropy constant (term in the hamiltonian -Kz*Sz^2 )
% jx        = current density
%
function [SxNext,SyNext,SzNext] = rk4Step(dt,Sx,Sy,Sz,a,b,J1,J2,Hx,Hy,Hz,Kz,jx)
    dt6 = dt/6.0;
    % computing the different interpolation points
    [k1X,k1Y,k1Z] = llgFunction(Sx,Sy,Sz,a,b,J1,J2,Hx,Hy,Hz,Kz,jx);
    [k2X,k2Y,k2Z] = llgFunction(Sx+0.5*k1X*dt,Sy+0.5*k1Y*dt,Sz+0.5*k1Z*dt,a,b,J1,J2,Hx,Hy,Hz,Kz,jx);
    [k3X,k3Y,k3Z] = llgFunction(Sx+0.5*k2X*dt,Sy+0.5*k2Y*dt,Sz+0.5*k2Z*dt,a,b,J1,J2,Hx,Hy,Hz,Kz,jx);
    [k4X,k4Y,k4Z] = llgFunction(Sx+k3X*dt,Sy+k3Y*dt,Sz+k3Z*dt,a,b,J1,J2,Hx,Hy,Hz,Kz,jx);
    % computing the weighted average
    SxNext = Sx + dt6*(k1X + 2.0*k2X + 2.0*k3X + k4X);
    SyNext = Sy + dt6*(k1Y + 2.0*k2Y + 2.0*k3Y + k4Y);
    SzNext = Sz + dt6*(k1Z + 2.0*k2Z + 2.0*k3Z + k4Z);
end
```

BIBLIOGRAPHY

[1] T. H. R. Skyrme. *Nucl. Phys.*, 31:556–569, 1962. doi: 10.1016/0029-5582(62)90775-7. URL http://dx.doi.org/10.1016/0029-5582(62)90775-7.

[2] A. N. Bogdanov and D. A. Yablonskii. Thermodynamically stable "vortices" in magnetically ordered crystals. the mixed state of magnets. *Sov. Phys. JETP*, 68:101–103, 1989.

[3] S. Mühlbauer. Skyrmion lattice in a chiral magnet. *Science*, 323: 915–919, 2009. doi: 10.1126/science.1166767. URL http://dx.doi.org/10.1126/science.1166767.

[4] X. Z. Yu et al. Real-space observation of a two-dimensional skyrmion crystal. *Nature*, 465:901–904, 2010. doi: 10.1038/nature09124. URL http://dx.doi.org/10.1038/nature09124.

[5] S. Heinze et al. *Nature Phys.*, 7:713–718, 2011. doi: 10.1038/nphys2045. URL http://dx.doi.org/10.1038/nphys2045.

[6] R. Rajamaran. *Solitons and Instantons*. 1987.

[7] H. B. Braun. *Adv. Phys.*, 26:1–116, 2012.

[8] T. Garel and S. Doniach. *Phys. Rev. B*, 26:325–329, 1982.

[9] S. V. Grigoriev et al. *Phys. Rev. Lett.*, 102:037204, 2009.

[10] X. Z. Yu et al. Near room-temperature formation of a skyrmion crystal in thin-films of the helimagnet fege. *Nat. Mater.*, 10:106–109, 2011. doi: 10.1038/nmat2916. URL http://dx.doi.org/10.1038/nmat2916.

[11] K. Shibata et al. *Phys. Rev. Lett.*, 8:723–728, 2013.

[12] T. Okubo, S. Chung, and H. Kawamura. *Phys. Rev. Lett.*, 108: 017206, 2012.

[13] N. S. Kiselev, A. N. Bogdanov, R. Schafer, and U. K. Rossler. *J. Phys. D*, 44:392001, 2011. doi: 10.1088/0022-3727/44/39/392001. URL http://dx.doi.org/10.1088/0022-3727/44/39/392001.

[14] S. S. P. Parkin, M. Hayashi, and L. Thomas. Magnetic domain-wall racetrack memory. *Science*, 320:190–194, 2008. doi: 10.1126/science.1145799. URL http://dx.doi.org/10.1126/science.1145799.

[15] F. Jonietz et al. Spin transfer torques in mnsi at ultralow current densities. *Science*, 330:1648–1651, 2010. doi: 10.1126/science.1195709. URL http://dx.doi.org/10.1126/science.1195709.

[16] Albert Fert, Vincent Cros, and Joao Sampaio. Skyrmions on the track. *Nat Nano*, 8(3):152–156, Mar 2013. ISSN 1748-3387. doi: 10.1038/nnano.2013.29. URL http://dx.doi.org/10.1038/nnano.2013.29.

[17] N. Romming et al. *Science*, 341:636–639, 2013.

[18] M. Mochizuki, X. Z. Yu, S. Seki, N. Kanazawa, W. Koshibae, J. Zang, M. Mostovoy, Y. Tokura, and N. Nagaosa. Thermally driven ratchet motion of a skyrmion microcrystal and topological magnon hall effect. *Nat Mater*, 13(3):241–246, Mar 2014. ISSN 1476-1122. URL http://dx.doi.org/10.1038/nmat3862. Letter.

[19] G. Tatara, H. Kohno, and J. Shibata. Microscopic approach to current-driven domain wall dynamics. *Phys. Rep.*, 468:213–301, 2008. doi: 10.1016/j.physrep.2008.07.003. URL http://dx.doi.org/10.1016/j.physrep.2008.07.003.

[20] Christian Pfleiderer and Achim Rosch. Condensed-matter physics: Single skyrmions spotted. *Nature*, 465(7300):880–881, Jun 2010. ISSN 0028-0836. doi: 10.1038/465880a. URL http://dx.doi.org/10.1038/465880a.

[21] A. Neubauer. Topological hall effect in the a phase of mnsi. *Phys. Rev. Lett.*, 102:186602, 2009. doi: 10.1103/PhysRevLett.102.186602. URL http://dx.doi.org/10.1103/PhysRevLett.102.186602.

[22] N. Nagaosa, X. Z. Yu, and Y Tokura. *Phil. Trans. R. Soc. A*, 370:5806–5819, 2012.

[23] J. Zang, M. Mostovoy, J. H. Han, and N. Nagaosa. Dynamics of skyrmion crystals in metallic thin films. *Phys. Rev. Lett.*, 107:136804, 2011. doi: 10.1103/PhysRevLett.107.136804. URL http://dx.doi.org/10.1103/PhysRevLett.107.136804.

[24] N. Nagaosa and Y. Tokura. Topological properties and dynamics of magnetic skyrmions. *Nat. Nano.*, 8(12):899–911, December 2013. doi: 10.1038/nnano.2013.243. URL http://dx.doi.org/10.1038/nnano.2013.243.

[25] I. E. Dzyaloshinskii. *J. Phys. Chem. Sol.*, 4:241–255, 1958. doi: 10.1016/0022-3697(58)90076-3. URL http://dx.doi.org/10.1016/0022-3697(58)90076-3.

[26] T. Moriya. *Phys. Rev.*, 120:91–98, 1960. doi: 10.1103/PhysRev.120.91. URL http://dx.doi.org/10.1103/PhysRev.120.91.

[27] K Everschore. *Current-Induced Dynamics of Chiral Magnetic Structures*. PhD thesis, der Universität zu Köln, 2012.

[28] T. Jeong and W. E. Pickett. Implications of the b20 crystal structure for the magnetoelectronic structure of MnSi. *Phys. Rev. B*, 70:075114, Aug 2004. doi: 10.1103/PhysRevB.70.075114. URL http://link.aps.org/doi/10.1103/PhysRevB.70.075114.

[29] U. K. Rößler, A. A. Leonov, and A. N. Bogdanov. Chiral skyrmionic matter in non-centrosymmetric magnets. *J. Phys.: Conf. Ser.*, 303:012105, 2011. doi: doi:10.1088/1742-6596/303/1/012105.

[30] A. B. Butenko, A. A. Leonov, U. K. Rößler, and A. N. Bogdanov. Stabilization of skyrmion textures by uniaxial distortions in noncentrosymmetric cubic helimagnets. *Phys. Rev. B*, 82:052403, 2010. doi: 10.1103/PhysRevB.82.052403. URL http://dx.doi.org/10.1103/PhysRevB.82.052403.

[31] M. N. Baibich et al. Giant magnetoresistance of (001)fe/(001)cr magnetic superlattices. *Phys. Rev. Lett.*, 61:2472, 1988.

[32] G. Binasch, P. GrÃŒnberg, F. Saurenbach, and W. Zinn. Enhanced magnetoresistance in layered magnetic structures with antiferromagnetic interlayer exchange. *Phys. Rev. B*, 39:4828, 1989.

[33] L. Berger. Emission of spin waves by a magnetic multilayer traversed by a current. *Phys. Rev. B*, 54:9353–9358, 1996. doi: 10.1103/PhysRevB.54.9353. URL http://dx.doi.org/10.1103/PhysRevB.54.9353.

[34] J. C. Slonczewski. Current-driven excitation of magnetic multilayers. *J. Magn. Magn. Mater.*, 159:L1–L7, 1996. doi: 10.1016/0304-8853(96)00062-5. URL http://dx.doi.org/10.1016/0304-8853(96)00062-5.

[35] M. V. Berry. Quantal phase factors accompanying adiabatic changes. *Proc. R. Soc. Lond. A*, 392(1802):45–57, 1984.

[36] M. Born and V. A. Fock. Beweis des adiabatensatzes. *Zeitschrift für Physik A*, 51:165–180, 1928. doi: doi:10.1007/BF01343193.

[37] P. Bruno, V. K. Dugaev, and Taillefumier M. Topological hall effect and berry phase in magnetic nanostructures. *Phys. Rev. Lett.*, 93:096806, 2004.

[38] G. Tatara et al. Spin torque and force due to current for general spin textures. *J. Phys. Soc. Jpn.*, 76:054707, 2007.

[39] A. A. Thiele. Steady-state motion of magnetic domains. *Phys. Rev. Lett.*, 30:230–233, 1972. doi: 10.1103/PhysRevLett.30.230. URL http://dx.doi.org/10.1103/PhysRevLett.30.230.

[40] J. Iwasaki, M. Mochizuki, and N. Nagaosa. *Nature Commun.*, 4: 1463, 2013. doi: 10.1038/ncomms2442. URL http://dx.doi.org/10.1038/ncomms2442.

COLOPHON

This document was typeset using the typographical look-and-feel `classicthesis` developed by André Miede. The style was inspired by Robert Bringhurst's seminal book on typography "*The Elements of Typographic Style*". `classicthesis` is available for both LaTeX and LyX:

http://code.google.com/p/classicthesis/

Happy users of `classicthesis` usually send a real postcard to the author, a collection of postcards received so far is featured here:

http://postcards.miede.de/

Final Version as of August 5, 2014 (`classicthesis` draft: version 4.0).

DECLARATION

I declare that this thesis and the work presented in it are my own and have been generated by me as the result of my own original research. Where other sources of information have been used, they have been acknowledged.

Groningen – The Netherlands, July 2014

Alessio Pozzi